

# 2

## Electromagnetic interactions

Before a particle can be detected, it must first undergo some sort of interaction in the material of a detector. Processes that result from the electromagnetic interaction are the most important for particle detection. In this chapter we will consider four major topics. The first is the loss of energy by charged particles heavier than the electron due to the excitation or ionization of atomic electrons. We will calculate the most probable value of the ionization energy loss and the distribution of the fluctuations in that quantity. Second, we will consider the interactions of electrons. These include ionization losses and the loss of energy due to photon emission (bremsstrahlung). The third topic is the interaction of photons with matter. The most important of these are the photoelectric effect, the Compton effect, and pair production. Lastly, we will examine Coulomb scattering of charged particles with the atomic nucleus, which is responsible for multiple scattering.

There are additional processes that, although they are electromagnetic in nature, are more appropriately discussed in other sections of the book. These include scintillation light (Chapter 7), Cerenkov light (Chapter 8), ionization in gases (Chapter 9), electromagnetic showers (Chapter 11), and transition radiation (Chapter 12). Strong and weak nuclear interactions of particles in matter are discussed in Chapter 3.

A rigorous treatment of electromagnetic effects requires calculations using QED. This theory describes the interactions in terms of the exchange and emission of photons. Since these calculations require special techniques and tend to be rather lengthy, we shall be content to present simple arguments for the processes under consideration and only quote QED results [1].

### 2.1 Energy loss in matter

Let us begin by considering the loss of kinetic energy of an incident charged particle due to its Coulomb interaction with charged particles in matter. We first give a semiclassical argument that demonstrates the physical causes of the energy loss. Let the incident particle have mass  $M$ , charge  $z_1 e$ , and velocity  $v_1$ . We assume it is interacting with a particle in the material with mass  $m$  and charge  $z_2 e$  and that the material particle is essentially at rest. We restrict ourselves to cases where only small momentum transfers are involved, so that the trajectory of the incident particle is not appreciably altered and the material particle only has a small recoil. The trajectory of the incident particle defines the axis of a cylinder as shown in Fig. 2.1. We consider the interaction with a particle in the cylindrical shell a distance  $b$  from the axis. The distance  $b$  is referred to as the impact parameter for the interaction.

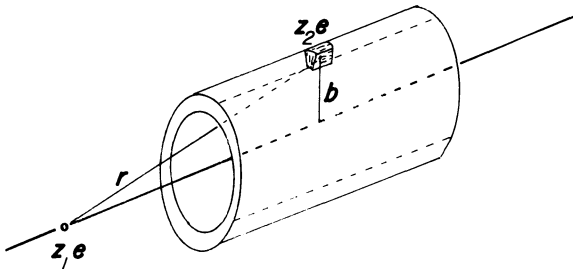
The moving charge creates an electric and magnetic field at the location of the material particle. Since the material particle is assumed to have only a small velocity, the magnetic interaction is not important. By symmetry the net force acting on the material particle is perpendicular to the cylinder. The transverse electric field is

$$\mathcal{E}_\perp = z_1 eb/r^3 \quad (2.1)$$

in the rest frame of the incident particle. The electric field observed in the LAB changes with time. Suppose that the incident particle reaches its point of closest approach at  $t = 0$ . At time  $t$  the transverse electric field in the LAB frame is given by [2]

$$\mathcal{E}_\perp = \frac{\gamma z_1 eb}{(b^2 + \gamma^2 v_1^2 t^2)^{3/2}} \quad (2.2)$$

**Figure 2.1** A cylindrical sheet of matter surrounding a particle trajectory.



The momentum acquired by the bound particle is

$$\begin{aligned}\Delta p &= \int F dt \\ &= \int_{-\infty}^{\infty} \frac{(z_2 e) \gamma z_1 e b dt}{(b^2 + \gamma^2 v_1^2 t^2)^{3/2}} \\ \Delta p &= \frac{2z_1 z_2 e^2}{v_1 b}\end{aligned}\tag{2.3}$$

The incident particle will have collisions with both the nuclei and the electrons of the atoms. Since the bound particle is assumed to have only a small velocity, the energy transfer can be written

$$\Delta E = \frac{(\Delta p)^2}{2m} = \frac{2z_1^2 z_2^2 e^4}{b^2 v_1^2 m}\tag{2.4}$$

We see that the energy transfer is inversely proportional to the square of the incident particle velocity and to the square of the impact parameter. Thus, most of the energy transfer is due to close collisions. We have  $m = m_e$  and  $z_2 = 1$  for electrons and  $m = Am_p$  and  $z_2 = Z$  for nuclei. With  $Z$  electrons in an atom and  $A \approx 2Z$ ,

$$\frac{\Delta E (\text{electrons})}{\Delta E (\text{nucleus})} = \frac{Z}{m_e} \left( \frac{Z^2}{2Zm_p} \right)^{-1} \approx 4000$$

so we see that the atomic electrons are responsible for most of the energy loss. We will let  $m = m_e$  for the rest of this chapter.

Now let us calculate the total energy lost by the incident particle per unit length in the material. We have just seen that most of the energy loss is due to interactions with the atomic electrons. There are  $n_e \times 2\pi b db dx$  electrons in the cylindrical shell of Fig. 2.1, where

$$n_e = Z_2 n_a = Z_2 \frac{N_A \rho}{A}\tag{2.5}$$

is the number of electrons per unit volume (cf. Appendix D). Summing over the total energy transfer in each  $b$  interval, the total energy loss per unit length is

$$\begin{aligned}dE/dx &= 2\pi n_e \left( \frac{2Z_1^2 e^4}{mv_1^2} \right) \int_{b_{\min}}^{b_{\max}} \frac{db}{b} \\ &= \frac{4\pi n_e Z_1^2 e^4}{mv_1^2} \ln \frac{b_{\max}}{b_{\min}}\end{aligned}\tag{2.6}$$

The limiting values of the impact parameter are determined by the

range of validity of the various assumptions that were made in deriving Eq. 2.6. We have assumed that the interaction takes place between the electric field of the incident particle and a free electron. However, the electron is actually bound to an atom. The interaction may be considered to be with a free electron only if the collision time is short compared to the characteristic orbital period of electrons in the atom. Examination of Eq. 2.2 shows that the transverse electric field in the LAB is very small except near  $t = 0$ . The full width at half maximum of the  $\mathcal{E}(t)$  distribution is  $b/v\gamma$  times a constant of order 1, so we take [2]

$$t_{\text{coll}} \approx \frac{b}{v_1\gamma} \quad (2.7)$$

An upper limit for the impact parameter then is

$$b_{\text{max}} \approx \frac{\gamma v_1}{\omega} \quad (2.8)$$

where  $\omega$  is a characteristic orbital frequency. A lower limit of validity for  $b$  is obtained from the requirement that  $\Delta E$  cannot exceed the maximum allowed energy transfer for a head-on collision. Thus, equating Eq. 2.4 evaluated at  $b_{\text{min}}$  with Eq. 1.24, we find that

$$b_{\text{min}} \approx \frac{Z_1 e^2}{\gamma m v_1^2} \quad (2.9)$$

If we substitute Eqs. 2.8 and 2.9 into Eq. 2.6, we obtain

$$\frac{dE}{dx} = \frac{4\pi n_e Z_1^2 e^4}{m v_1^2} \ln \frac{m v_1^3 \gamma^2}{Z_1 e^2 \omega} \quad (2.10)$$

A more rigorous classical calculation, originally due to Bohr, treats the atom as a harmonically bound charge for distant collisions. However, the results of this calculation differ numerically from Eq. 2.10 by a negligible amount [2].

Now let us determine the classical electromagnetic cross section for an incident particle to lose an amount of energy  $W$ . Consider a ring of width  $db$  at an impact parameter  $b$  from an atom. Every incident particle passing through the annular region undergoes a certain deflection. By definition, the differential cross section is the area of the ring and

$$\frac{d\sigma(b)}{db} db = 2\pi b db$$

We use Eq. 2.4 to relate  $b$  to the energy transferred to an atomic electron, which we assume is equal to the energy  $W$  lost by the incident particle. We find that

$$\begin{aligned}\frac{d\sigma}{db} db &= \frac{2\pi Z_1^2 Z_2^2 e^4}{mv_1^2} \frac{dW}{W^2} \\ &= \frac{d\sigma(W)}{dW} dW\end{aligned}$$

Thus, the classical cross section for obtaining an energy loss  $W$  is

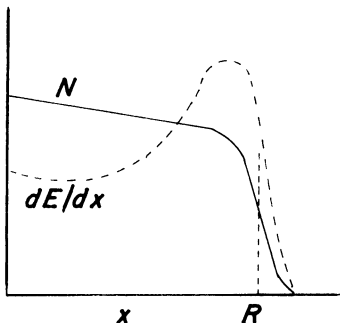
$$\frac{d\sigma}{dW} = \frac{2\pi Z_1^2 Z_2^2 e^4}{mv_1^2 W^2} \quad (2.11)$$

When electromagnetic scattering represents the dominant source of energy loss, a pure beam of monoenergetic, charged, stable particles heavier than the electron travels approximately the same range  $R$  in matter. For example, a beam of 1 GeV/c protons has a range of about 200 g/cm<sup>2</sup> in lead (17.6 cm). Because of their light mass, the paths of electrons in matter have much larger deviations. A plot of the number of heavy charged particles in a beam is shown in Fig. 2.2 as a function of the depth into the material. Also shown is the local value of  $dE/dx$ . The small decrease in intensity that occurs at all depths is caused by nuclear or large angle scattering processes. An interaction that removes particles of a given type from a beam leads to an exponential decrease in the intensity of those particles. Most of the ionization loss occurs near the end of the path, where the velocity is smallest. This increase in the energy loss is referred to as the Bragg peak. The depth at which half the initial particles remain is called the mean range. This is related to the energy loss by

$$R(E) = \int_E^0 \frac{1}{-dE/dx} dE \quad (2.12)$$

The range represents the distance traversed along the trajectory of the

**Figure 2.2** Number of heavy charged particles in a beam and  $dE/dx$  as a function of depth in the absorber ( $R$  is the mean range).



particle itself and differs from the thickness of the absorber because of multiple scattering.

We can derive an important scaling law for the range. The energy loss formula can be written

$$\frac{dE}{dx} = Z_1^2 f(v) = Z_1^2 g\left(\frac{E}{M}\right)$$

where  $f$  and  $g$  are functions. Then, according to Eq. 2.12, the range is given by an equation of the form

$$R = \int \frac{1}{Z_1^2 g(E/M)} M \frac{dE}{M} \quad (2.13)$$

$$R\left(\frac{E}{M}\right) = \frac{M}{Z_1^2} h\left(\frac{E}{M}\right)$$

where  $h$  is a universal function of  $E/M$ . To illustrate the usefulness of Eq. 2.13, suppose that the range of some particle, a proton, for example, has been measured as a function of  $v$  or of  $E/M$ . Then the range of another particle, an alpha particle, for example, with energy  $E_\alpha$  can be related to the proton range by

$$\frac{Z_p^2}{M_p} R_p\left(\frac{E_\alpha}{M_\alpha}\right) = \frac{Z_\alpha^2}{M_\alpha} R_\alpha\left(\frac{E_\alpha}{M_\alpha}\right)$$

$$R_\alpha\left(\frac{E_\alpha}{M_\alpha}\right) = \frac{M_\alpha}{M_p} \frac{Z_p^2}{Z_\alpha^2} R_p\left(\frac{E_\alpha}{M_\alpha}\right)$$

The range–energy relation can often be expressed empirically in the form

$$R(E) = (E/E_0)^n \quad (2.14)$$

For example, the range in meters for low energy protons in air can be approximated with  $n = 1.8$  and  $E_0 = 9.3$  MeV [3].

The energy losses and ranges of a number of incident particles in a variety of absorber materials are shown in Fig. 2.3. The range and  $dE/dx$  are expressed in terms of the amount of mass traversed ( $\text{g}/\text{cm}^2$ ) instead of the linear distance. All the  $dE/dx$  curves show the  $1/v^2$  drop for small momentum and a region of minimum ionization for higher momentum. Similar curves are given for particles in liquid hydrogen in Fig. 2.4.

## 2.2 Quantum treatment of the energy loss

The semiclassical treatment of the energy loss given in the preceding section treats the quantum nature of the particles in an ad hoc fashion. A proper treatment must take into account (1) the fact that

**Figure 2.3** Mean range and energy loss of charged particles in solids. Calculations use the Bethe–Bloch equation with density effect corrections. Refer to the cited reference for a discussion of assumptions and qualifications. (Particle Data Group, Rev. Mod. Phys. 56: S1, 1984.)

**PARTICLE DETECTORS, ABSORBERS, AND RANGES**

**Mean Range and Energy Loss in Lead, Copper, Aluminum, and Carbon**

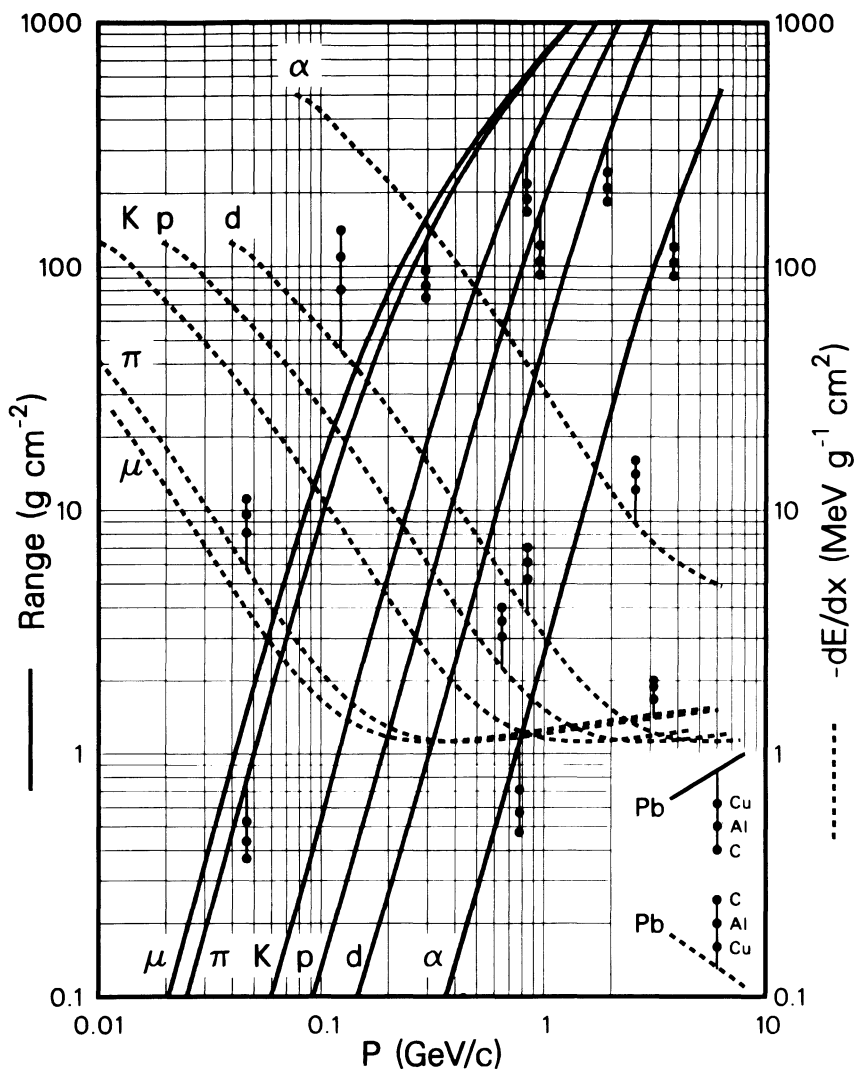
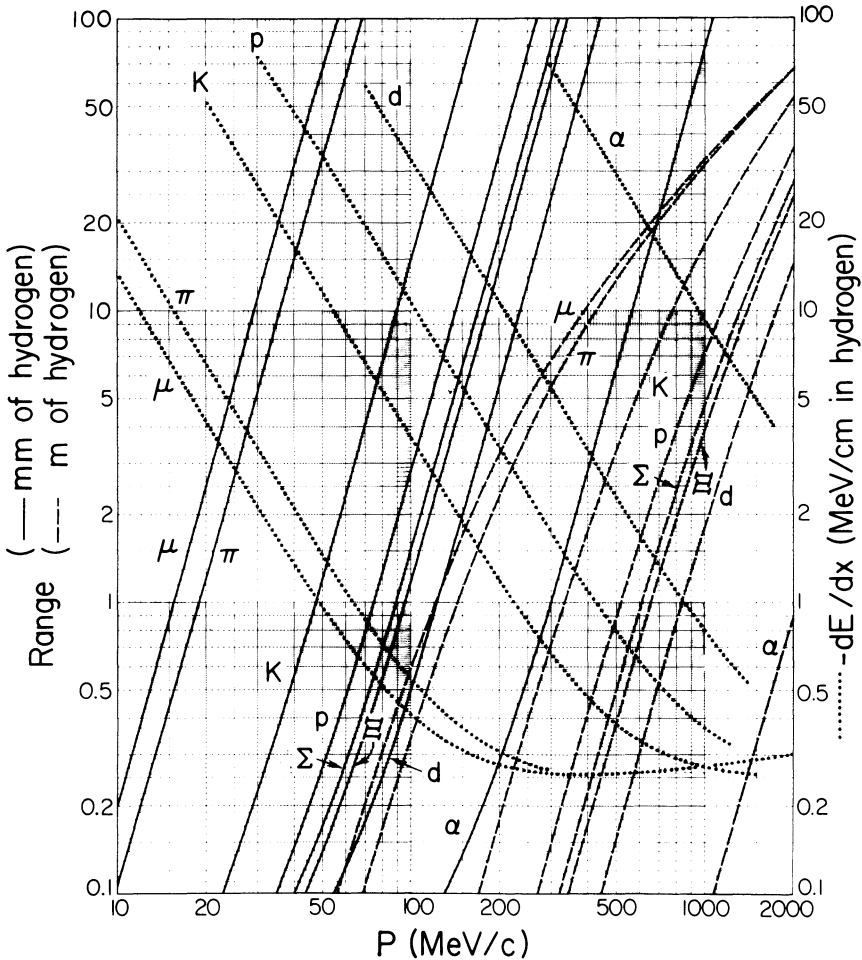


**Figure 2.4** Mean range and energy loss of charged particle in liquid hydrogen. Calculations use the Bethe–Bloch equation with density-effect corrections. Refer to the cited reference for a discussion of assumptions and qualifications. (Particle Data Group, Rev. Mod. Phys. 56: S1, 1984.)

**PARTICLE DETECTORS, ABSORBERS, AND RANGES**

**Mean Range and Energy Loss in Liquid Hydrogen**





energy transfers to the atomic electrons only occur in discrete amounts and (2) the wave nature of the particles. For very close collisions the classical specification of a particle as an object with a well-defined position and momentum conflicts with the uncertainty principle. In the early 1930s Bethe and Bloch treated the problem of energy loss in the framework of quantum mechanics. We will summarize some important aspects of their treatment in this section [4, 5].

Bethe's theory classifies atomic collisions according to the amount of momentum or energy transfer to the bound electron. This is an observable quantity in contrast to the impact parameter used in the semiclassical derivation. However, one can associate the small momentum transfer processes with a large impact parameter (distant collisions) and the large momentum transfers with small impact parameters (close collisions).

In distant collisions the incident particle interacts with the atom as a whole. There will be a certain probability that the energy lost by the incident particle will cause excitation of an electron to a higher energy level or will cause ionization. Bethe calculated the probabilities for these transitions using first-order perturbation theory. The incident particle is treated as a plane wave. The spin and magnetic moment of the atomic electrons are properly treated if Dirac wavefunctions are used. The perturbation is the Coulomb potential plus a coupling to the photon field. The total contribution to the energy loss comes from summing all excitation energies, each weighted by the cross section for that excitation. Thus,

$$\left. \frac{dE}{dx} \right|_{w < \eta} = n_a \sum_n \int E_n d\sigma_n \quad (2.15)$$

where  $\eta$  is a limiting energy transfer ( $\sim 50$  KeV) for which the assumptions used in deriving Eq. 2.15 are valid [1]. The expression obtained after evaluating Eq. 2.15 depends on the atomic properties through the mean ionization potential  $I$ .

For close collisions the interaction can be considered to be with free electrons, and atomic properties are not involved. The energy loss due to close collisions can be written

$$\left. \frac{dE}{dx} \right|_{w > \eta} = n_e \int_{\eta}^{w_{\max}} W \frac{d\sigma}{dW}(E, W) dW \quad (2.16)$$

Note that  $(d\sigma/dW)(E, W)$  is the cross section for an incident particle with energy  $E$  to lose an amount of energy  $W$  in the collision with a free electron. The cross section depends on the type of incident particle. For spin 0 particles heavier than the electron, the differential cross section is given by [1]

$$\frac{d\sigma}{dW}(E, W) = 2\pi \frac{e^4}{mc^2} \frac{1}{\beta^2 W^2} \left( 1 - \beta^2 \frac{W}{W_{\max}} \right) \quad (2.17)$$

while for heavy spin  $\frac{1}{2}$  incident particles

$$\frac{d\sigma}{dW}(E, W) = 2\pi \frac{e^4}{mc^2} \frac{1}{\beta^2 W^2} \left[ 1 - \beta^2 \frac{W}{W_{\max}} + \frac{1}{2} \left( \frac{W}{E + mc^2} \right)^2 \right] \quad (2.18)$$

When  $W \ll W_{\max}$ , both of these cross sections reduce to that for Coulomb scattering, Eq. 2.11. Thus, for small energy transfers the cross sections only depend on the energy of the recoiling electron and the velocity of the incident particle. Spin only plays an important role when  $W \sim E$ .

The total energy loss is the sum of the contributions from close and distant collisions. The result for the energy loss of a heavy, spin 0 incident particle is [5]

$$\frac{dE}{dx} = \frac{4\pi n_e Z_1^2 e^4}{mv_1^2} \left( \ln \frac{2mv^2\gamma^2}{I} - \beta^2 \right) \quad (2.19)$$

It is important to note that the final expression for the energy loss does not depend on the intermediate energy transfer  $\eta$  used to separate the classes of collisions.

It is useful to break up the constant in front of Eq. 2.19 into separate factors relating to the incident particle, the material medium, and the intrinsic properties of the electron. First recall that the electron's charge is related to the so-called classical radius of the electron by

$$r_e = e^2/(mc^2) \quad (2.20)$$

Using Eqs. 2.5 and 2.20, the fixed constants and electron properties can be combined into the constant

$$\begin{aligned} D_e &= 4\pi r_e^2 mc^2 \\ &= 5.0989 \times 10^{-25} \text{ MeV-cm}^2 \end{aligned} \quad (2.21)$$

Equation 2.19 can then be written in the convenient form

$$\frac{dE}{dx} = D_e \left( \frac{Z_1}{\beta_1} \right)^2 n_e \left[ \ln \frac{2mc^2\beta^2\gamma^2}{I} - \beta^2 \right] \quad (2.22)$$

Now let us consider the important features of Eq. 2.22. The energy loss depends quadratically on the charge and velocity of the incident particle, but not on its mass. Thus, for a beam of particles with a given charge, the energy loss is a function of the velocity only. The energy loss depends on the material linearly through the electron density factor  $n_e$  and logarithmically through the mean ionization potential  $I$ .

As the velocity of the particle increases from near zero,  $dE/dx$  falls due to the  $1/v^2$  factor. All incident particles have a region of minimum ionization with  $dE/dx \sim 2 \text{ MeV/g cm}^2$  for  $\beta\gamma \approx 3$ . As  $\beta$  continues to increase,

the  $\ln \gamma^2$  factor in Eq. 2.22 begins to dominate and  $dE/dx$  starts to increase. This is referred to as the region of relativistic rise. In the semiclassical picture the relativistic deformation of the Coulomb field of the incident particle increases the upper limit for impact parameters involved in the collision (see Eq. 2.8).

The mean ionization potential per electron depends on the atomic number of the atom. Bloch used the Thomas–Fermi model of the atom to show that  $I$  should vary linearly with  $Z$ . An approximate expression is

$$I/Z \approx 10 \text{ eV} \quad (2.23)$$

which is generally valid for  $Z \geq 20$ . Numerical values for the mean ionization potential of some materials are given in Table 2.1.

Table 2.1. *Electromagnetic properties of elements<sup>a</sup>*

Material	$Z$	$n_a$ ( $\times 10^{23}/\text{cm}^3$ )	$n_e$ ( $\times 10^{23}/\text{cm}^3$ )	$I$ (eV)	$L_R$ (cm)	$X_R$ ( $\text{g}/\text{cm}^2$ )	Density ( $\text{g}/\text{cm}^3$ )
H <sub>2</sub>	1	0.423	0.423	21.8	891	63.05	0.0708
He	2	0.188	0.376	41.8	755	94.32	0.125
Li	3	0.463	1.39	40.0	155	82.76	0.534
Be	4	1.23	4.94	63.7	35.3	65.19	1.85
B	5	1.32	6.60	76	22.2	52.69	2.37
C	6	1.146	6.82	78	18.8	42.70	2.27
N <sub>2</sub>	7	0.347	2.43	85.1	47.0	37.99	0.808
O <sub>2</sub>	8	0.429	3.43	98.3	30.0	34.24	1.14
Ne	10	0.358	3.58	137 <sup>b</sup>	24.0	28.94	1.20
Al	13	0.603	7.84	166	8.89	24.01	2.70
Si	14	0.500	6.99	173	9.36	21.82	2.33
Ar	18	0.211	3.80	188 <sup>b</sup>	14.0	19.55	1.40
Fe	26	0.849	22.1	286	1.76	13.84	7.87
Cu	29	0.845	24.6	322	1.43	12.86	8.92
Zn	30	0.658	19.6	330	1.75	12.43	7.14
Kr	36	0.155	5.59	352 <sup>b</sup>	5.26	11.37	2.16
Ag	47	0.586	27.6	470	0.85	8.97	10.5
Sn	50	0.371	18.5	488	1.21	8.82	7.31
W	74	0.632	46.8	727	0.35	6.76	19.3
Pt	78	0.662	51.5	790	0.31	6.54	21.45
Au	79	0.577	45.6	790	0.34	6.46	18.88
Pb	82	0.330	27.0	823	0.56	6.37	11.34
U	92	0.479	44.1	890	0.32	6.00	18.95

<sup>a</sup> Values are for solid and liquid states unless noted.

<sup>b</sup> Gaseous state.

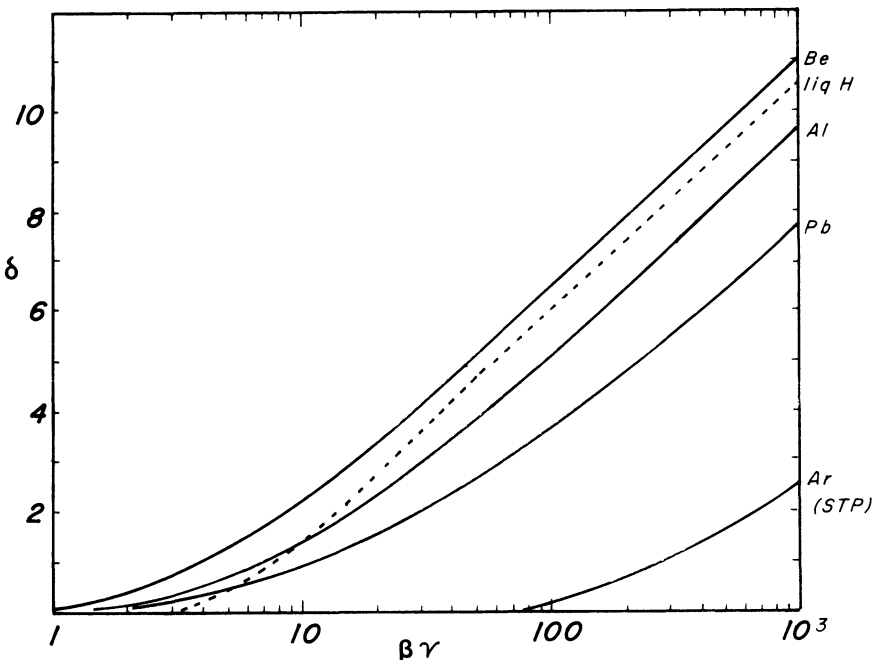
Source: Particle Data Group, Rev. Mod. Phys. 56: S1, 1984, S53; S. Ahlen, Rev. Mod. Phys. 52: 121, 1980, Table 6; Y. Tsai, Rev. Mod. Phys. 46: 815, 1974, Table 3.6; *Handbook of Chemistry and Physics*, 64th ed., Boca Raton: CRC Press, 1983, p. B65; R.M. Sternheimer, M.J. Berger, and S.M. Seltzer, Atomic Data and Nuclear Data Tables 30: 261, 1984, Table 1.

The relativistic rise does not continue indefinitely. The theory we have described so far treats the interaction of the incident particle with an isolated atom. However, for dense materials where the interatomic spacing is small, the upper limit on allowed impact parameters may encompass many atoms. In this case interactions among the atomic electrons can cause a screening of the projectile's electric field. Fermi developed a theory of dielectric screening that explains the reduction of energy loss for distant collisions [4]. This phenomenon is known as the density effect since it is affected by the density of the medium. It causes the energy loss in the region of relativistic rise to only increase like  $\ln \gamma$  instead of  $\ln \gamma^2$  and causes the loss to become constant at very large  $\gamma$ . The constant ionization loss at large  $\gamma$  is referred to as the Fermi plateau.

Taking the density effect into account, the energy loss formula can be written

$$\frac{dE}{dx} = D_e \left( \frac{Z_1}{\beta_1} \right)^2 n_e \left[ \ln \frac{2mc^2\beta^2\gamma^2}{I} - \beta^2 - \frac{\delta(\gamma)}{2} \right] \tag{2.24}$$

**Figure 2.5** Density effect correction parameter  $\delta$  for several materials. (The parameter was calculated using the formulas and coefficients given in R.M. Sternheimer, M.J. Berger, and S.M. Seltzer, Atomic Data and Nuclear Data Tables 30: 261, 1984.)

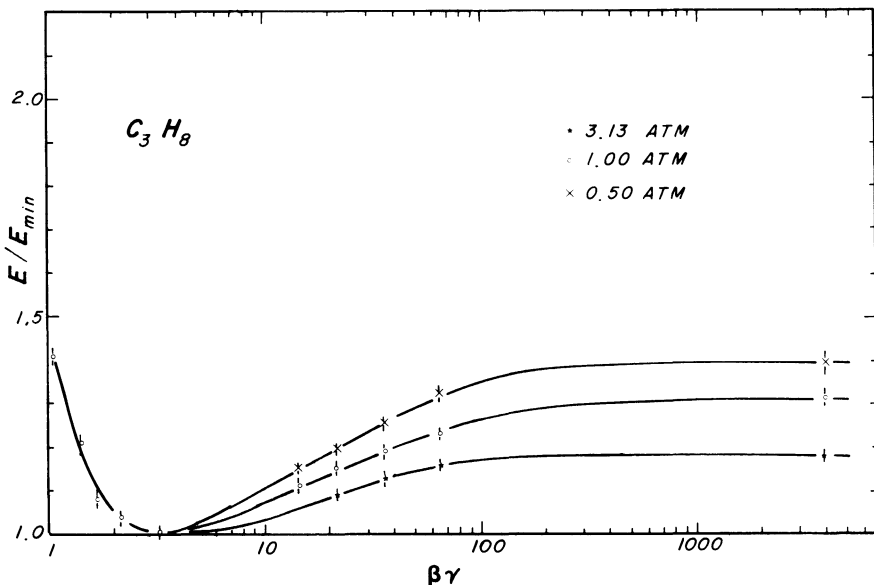


where  $\delta(\gamma)$  is a correction due to the density effect. A successful model for calculating  $\delta$  in terms of atomic properties has been developed by Sternheimer. Formulas giving the correction in terms of the ionization potential and the plasma frequency of the material can be found in Sternheimer's papers [6]. Values of  $\delta$  for several materials are shown in Fig. 2.5. The density effect correction changes the calculated ionization loss by  $\sim 15\%$  for particles with  $\beta\gamma = 100$  in metals. Note that nonconductors have a sharp threshold in  $\beta\gamma$ .

Measurements of  $dE/dx$  in propane are shown in Fig. 2.6 as a function of  $\beta\gamma$  and the gas pressure [7]. The measurements were made by collecting the charge liberated by ionization in a proportional chamber. Note that the plateau value of  $dE/dx$  at large  $\beta\gamma$  decreases with increasing pressure due to the density effect. Measurements [8] of the ionization losses of high energy protons and pions in high pressure hydrogen gas have also shown that the energy loss in the Fermi plateau remains constant for  $\gamma$  values as high as 1800.

One should keep in mind that the derivation of the energy loss expression given in Eq. 2.19 makes use of a number of simplifying assumptions.

**Figure 2.6** Measured mean energy losses in propane as a function of pressure and  $\beta\gamma$ . The energy losses are normalized to those for 3-GeV/ $c$  protons. (After A. Walenta, J. Fischer, H. Okuno, and C. Wang, *Nuc. Instr. Meth.* 161: 45, 1979.)



At the low  $\beta$  extreme atomic shell corrections are necessary when the velocity of the incident particle becomes comparable to the velocity of the bound electrons. On the other hand, at large  $\gamma$  radiation, kinematic, and incident particle structure corrections may be necessary [5]. One should also remember that excitation and ionization are not the only causes of energy loss. At large  $\gamma$  other contributing processes include Cerenkov radiation, transition radiation, bremsstrahlung, and pair production.

### 2.3 Fluctuations in energy loss

The amount of energy lost by a charged particle that has traversed a fixed thickness of absorber will vary due to the statistical nature of its interactions with individual atoms in the material. The value of  $dE/dx$  calculated in the preceding section is an averaged value. We have seen in Eq. 2.11 that collisions with small energy transfers are more likely than those with large transfers. Thus, the most probable energy loss will be shifted to the lower half of the range of possible energy transfers. The large energy transfer events are associated with the production of high energy recoil electrons (and from nuclear interactions). The result is that the energy loss distribution will be asymmetric with a tail on the high energy side.

For historical reasons the high energy recoil electrons are called delta rays. The number of delta rays produced with energy greater than  $E_1$  in a thickness  $x$  is

$$N(E \geq E_1) = \int_{E_1}^{E_{\max}} \xi \frac{dE}{E^2} \quad (2.25)$$

where

$$\xi = \frac{2\pi n_e Z_1^2 e^4}{mv^2} x \quad (2.26)$$

and  $E_{\max}$  is the maximum possible energy transfer. Thus,

$$N(E \geq E_1) = \xi \left( \frac{1}{E_1} - \frac{1}{E_{\max}} \right) \quad (2.27)$$

So long as  $E_1 \ll E_{\max}$ , we see that the number of energetic delta rays falls off inversely with the energy and that the parameter  $\xi$  is the energy above which there will be, on the average, one delta ray produced. As such, it represents a “typical” value of the energy loss in the material.

The probability that an incident particle with energy  $E$  will lose energy between  $W$  and  $W + dW$  while traversing an infinitesimal thickness  $dx$  of absorber is (see Appendix D)

$$\phi(W) dW dx = n_a \frac{d\sigma(W)}{dW} dW dx \quad (2.28)$$

where  $d\sigma/dW$  is the differential cross section for the incident particle to lose energy  $W$  in a single collision with an absorber atom. The total probability of a collision in the thickness  $dx$ , regardless of the energy transfer, is  $q dx$  where

$$q = n_a \int_0^\infty d\sigma/dW dW \quad (2.29)$$

The quantity  $q$  is called the primary ionization rate.

Although the probability for an energy loss  $W$  in an infinitesimal absorber layer is given trivially by Eq. 2.28, the calculation of the corresponding probability for a finite thickness can be very complicated. Consider a beam of  $N$  particles all having energy  $E$ . Let  $\chi(W, x) dW$  be the probability that a particle loses an energy between  $W$  and  $W + dW$  after crossing a thickness  $x$  of absorber. The form of  $\chi$  may be determined by considering how it changes if the particles traverse an additional infinitesimal thickness  $dx$  in the absorber. The number of particles with energy losses between  $W$  and  $W + dW$  increases because some particles with energy loss less than  $W$  at  $x$  will undergo a collision in  $dx$  that increases its loss to between  $W$  and  $W + dW$ . On the other hand, the number of particles with energy losses between  $W$  and  $W + dW$  decreases because some particles in the correct interval will undergo a collision in  $dx$  and increase the total energy loss above  $W + dW$ . We assume that successive collisions are statistically independent, that the absorber medium is homogeneous, and that the total energy loss is small compared to the particles' incident energy. Then we can express the change in the number of particles as

$$N\chi(W, x + dx) dW - N\chi(W, x) dW = N \int_0^\infty \chi(W - \epsilon, x) \phi(\epsilon) dW dx d\epsilon - N\chi(W, x) dW q dx \quad (2.30)$$

Thus  $\chi$  satisfies the equation

$$\frac{\partial\chi(W, x)}{\partial x} = \int_0^\infty \phi(\epsilon)\chi(W - \epsilon, x) d\epsilon - q\chi(W, x) \quad (2.31)$$

A number of investigators have determined solutions to Eq. 2.31. The differences in the treatments arise chiefly from different assumptions made about the single collision energy transfer probability  $\phi(W)$ . Landau used the classical free electron cross section given in Eq. 2.11. He assumed

that a typical energy loss was (1) large compared to the binding energy of the electrons in the material, yet (2) small compared to the maximum possible energy loss. With these assumptions the function  $\chi$  can be factorized into the form [9, 10]

$$\chi(W, x) = \frac{1}{\xi} f_L(\lambda)$$

where

$$\lambda = \frac{1}{\xi} \left[ W - \xi \left( \ln \frac{\xi}{\epsilon'} + 1 - C_E \right) \right]$$

$$\ln \epsilon' = \ln \frac{(1 - \beta^2) I^2}{2mv^2} + \beta^2 \quad (2.32)$$

$$C_E = 0.577 \quad (\text{Euler's constant})$$

and  $\xi$  is given by Eq. 2.26. The quantity  $\epsilon'$  is the low energy cutoff of possible energy losses. It was chosen by Landau so that the mean energy loss agreed with the Bethe–Bloch theory.

The universal function  $f_L(\lambda)$  can be expressed in terms of the integral

$$f_L(\lambda) = \frac{1}{\pi} \int_0^\infty \exp[-u(\ln u + \lambda)] \sin \pi u \, du \quad (2.33)$$

The most probable value of the energy loss is given by [5]

$$W_{\text{mp}} = \xi \left( \ln \frac{\xi}{\epsilon'} + 0.198 - \delta \right) \quad (2.34)$$

where  $\delta$  is the density effect correction used in Eq. 2.24. The full width at half maximum of the distribution is

$$\text{FWHM} = 4.02\xi \quad (2.35)$$

It is convenient to use the quantity  $\xi/E_{\text{max}}$  to classify various theories of energy losses. Landau's second assumption mentioned above requires  $\xi/E_{\text{max}} \lesssim 0.01$ . In this case the number of delta rays with energies near  $E_{\text{max}}$  is very small, and single large energy loss events give an asymmetric high energy tail to the energy loss distribution. Landau's first assumption breaks down in very thin absorbers such as gases, where the typical loss may be comparable to the electron binding energy in the gas atoms. Experimental energy loss distributions for gases are broader than predicted by the Landau theory. Accurate treatment of the energy loss requires that the theory take into account the presence of discrete atomic energy levels [9].

The distributions approach a Gaussian for  $\xi/E_{\text{max}} \gtrsim 1$ . In this case the



number of delta rays observed with energy near  $E_{\max}$  is large. The most probable energy loss is also large, and the high energy loss events tend to average out. The width of the Gaussian is given simply by [5]

$$\sigma_w^2 = 4\pi Z_1^2 Z_2 n_a e^4 x \quad (2.36)$$

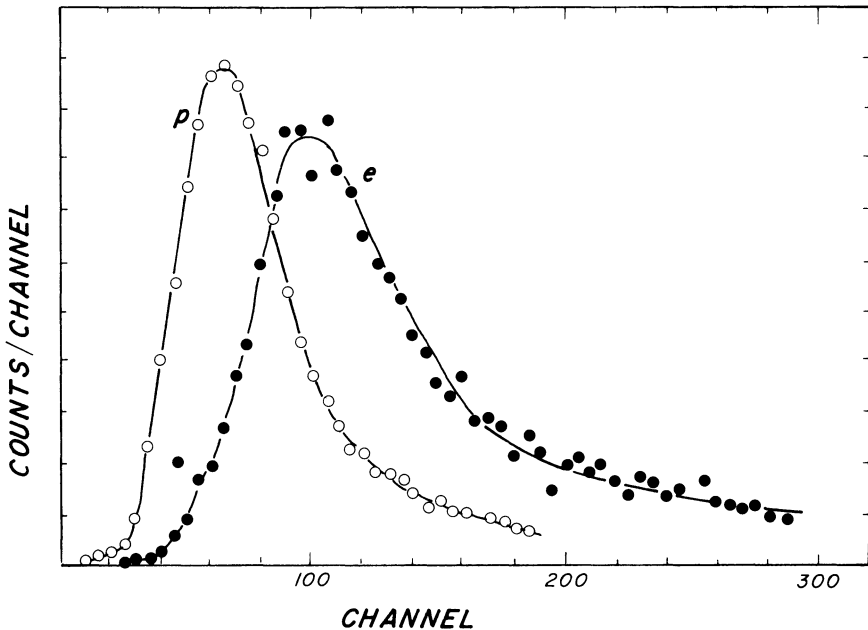
Vavilov has developed a theory for the intermediate case  $0.01 \approx \xi/E_{\max} \approx 1$  using the physical upper limit for the maximum energy transfer [11].

The pulse height spectra of high energy protons and electrons in a gaseous proportional chamber are shown in Fig. 2.7. It is clear that the most probable value of the energy loss is skewed to the low energy side of the asymmetric energy loss distribution.

Because of fluctuations in energy loss, a beam of particles of fixed energy will have a distribution of ranges in a thick absorber. This phenomenon is known as straggling. The two fluctuations are related by

$$\langle (E - \bar{E})^2 \rangle = \left( \frac{dE}{dx} \right)^2 \langle (R - \bar{R})^2 \rangle \quad (2.37)$$

**Figure 2.7** Measured pulse height distributions for 3-GeV/c protons and 2-GeV/c electrons in a 90% Ar + 10% CH<sub>4</sub> gas mixture. (After A. Walenta, J. Fischer, H. Okuno, and C. Wang, *Nuc. Instr. Meth.* 161: 45, 1979.)



Calculations of straggling have shown that the range distributions for protons in various metals are nearly Gaussian [5]. For a pure, monoenergetic beam of particles the fractional straggling  $\sigma_R/R$  increases with increasing  $Z$  of the absorber. The fractional straggling in a given absorber decreases with increasing kinetic energy and approaches a value  $\sigma_R/R \sim \frac{1}{2}(m/M)^{1/2}$  at high energy, where  $M$  is the mass of the incident particle.

## 2.4 Energy loss of electrons and positrons

Electrons and positrons lose energy by ionization just as the heavier charged particles do. However, because of their small mass, they also have significant losses due to the production of radiation. For lead the fractional energy loss due to bremsstrahlung exceeds that due to ionization for electron energies above 10 MeV. Other significant sources of energy loss for low energy electrons are elastic scattering and positron annihilation. For high energy electrons the bremsstrahlung and pair production processes lead to the production of electromagnetic showers.

Electrons and positrons have similar electromagnetic interactions in matter. Most of the statements we will make about electrons apply to positrons as well. When this is not the case, we will explicitly say so.

### 2.4.1 Ionization energy loss

The portion of the ionization loss resulting from distant collisions is the same for all incident particles. On the other hand, the portion resulting from close collisions depends on the form of the free electron cross section of the incident particle (Eq. 2.16). The differential cross section for the relativistic scattering of an electron from a free electron was first calculated by Moller. The cross section for finding a scattered electron with kinetic energy between  $W$  and  $W + dW$  is [12]

$$\frac{d\sigma}{dW} = \frac{2\pi e^4}{mv^2} \left[ \frac{1}{W^2} - \frac{1}{W(E-W)} \frac{mc^2(2E+mc^2)}{(E+mc^2)^2} + \frac{1}{(E-W)^2} + \frac{1}{(E+mc^2)^2} \right] \quad (2.38)$$

where  $E$  is the kinetic energy of the incident electron. The energy loss for relativistic electrons using this cross section is

$$\frac{dE}{dx} = \frac{2\pi n_e e^4}{mc^2} \left( 2 \ln \frac{2mc^2}{I} + 3 \ln \gamma - 1.95 \right) \quad (2.39)$$

The energy loss for positrons differs slightly since the Bhabha differential cross section must be used in place of the Moller cross section. The

corresponding expression for the energy loss of singly charged, heavy particles traveling at relativistic velocities can be found by evaluating Eq. 2.19 for  $\beta \rightarrow 1$

$$\frac{dE}{dx} = \frac{2\pi n_e e^4}{mc^2} \left( 2 \ln \frac{2mc^2}{I} + 4 \ln \gamma - 2 \right) \quad (2.40)$$

Comparison of Eqs. 2.39 and 2.40 shows that to first order all singly charged particles with  $\beta \sim 1$  lose energy by collisions at approximately the same rate. The second terms indicate that the rate of relativistic rise for electrons will be slightly smaller than for heavier particles.

Because of their small mass, electrons follow a very irregular path through matter. For this reason, the range for electrons has a wider distribution than the range for heavier particles. The mean range for 1-MeV electrons varies from about 0.22 g/cm<sup>2</sup> in hydrogen to 0.78 g/cm<sup>2</sup> in lead [13].

#### 2.4.2 Bremsstrahlung

The dominant energy loss mechanism for high energy electrons is the production of electromagnetic radiation. This is usually referred to as synchrotron radiation for circular acceleration and bremsstrahlung for motion through matter. Conservation of energy requires that  $E_i = E_f + k$ , where  $E_i$  ( $E_f$ ) is the initial (final) energy of the electron and  $k$  is the energy of the produced photon. The time rate of energy loss depends quadratically on the acceleration experienced by the particle through the well-known relation

$$dE/dt = (2e^2/3c^3)a^2 \quad (2.41)$$

where  $a$  is the acceleration.

A semiclassical calculation of the bremsstrahlung cross section for a relativistic particle gives [2]

$$\frac{d\sigma}{dk} \simeq 5 \frac{e^2}{\hbar c} Z_1^4 Z_2^2 \left( \frac{mc}{Mv_1} \right)^2 \frac{r_e^2}{k} \ln \frac{Mv_1^2 \gamma^2}{k} \quad (2.42)$$

We note that the cross section depends inversely on the square of the incident particle mass  $M$ . It is for this reason that up to the present date radiation energy loss has only been important for electrons and very high energy muons. The cross section depends on the medium through the factor  $Z_2^2$ , implying that heavy elements are most efficient at causing energy loss by radiation. Recall that ionization energy loss was proportional to  $Z_2$ . Finally note that the cross section falls off with increasing photon energy roughly as  $1/k$ .

Interactions of the incident particle with the Coulomb field of the nucleus go like  $Z_2^2$ . There is also a contribution from the atomic electrons that goes like  $Z_2$ . Thus, for all but the lightest elements the bremsstrahlung cross section is dominated by interactions with the nucleus. However, the atomic electrons cause another important effect by screening the nuclear charge. Classically, when the impact parameter is larger than the atomic radius, we expect the cross section to fall sharply since the effective charge seen by the incident particle is greatly reduced. This case is referred to as complete screening. The effect is also true quantum mechanically since one may define an “effective distance” of the electron from the nucleus  $\hbar/q$ , where  $q$  is the momentum transfer from the electron to the nucleus.

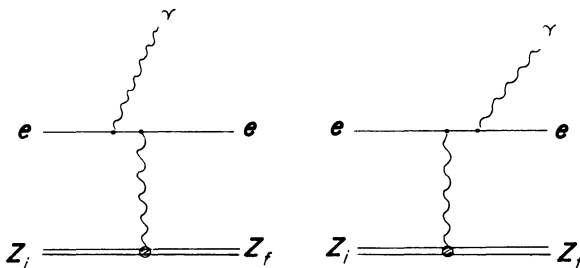
The results of QED calculations for the bremsstrahlung process can be found in a review by Tsai [14]. At least one virtual photon must be exchanged to the target system in order to conserve 4-momentum. The lowest-order QED diagrams shown in Fig. 2.8 do not depend on the sign of the charge of the lepton. Thus, we expect the same cross section from incident electrons and positrons. The interaction of the virtual photon with the target system depends on properties of the target, such as its mass, internal structure, spin, and screening of the nuclear charge by atomic electrons.

Bethe and Heitler made a quantum mechanical calculation of the bremsstrahlung cross section for an electron in the field of an infinitely heavy, pointlike, spinless nucleus [15]. The calculation makes use of the Born approximation, which is valid if

$$\frac{2\pi Z_2 e^2}{\hbar v} \ll 1 \tag{2.43}$$

where  $v$  can be the velocity of the electron before or after the photon emission. This relation is generally satisfied for energetic particles, except possibly for the heavy elements.

**Figure 2.8** Lowest-order Feynman diagrams for bremsstrahlung.



The effects of screening are determined by the parameter [12]

$$\begin{aligned}\Gamma &= \frac{100mc^2}{Z_2^{1/3}} \frac{k}{E_i E_f} \\ &= \frac{100mc^2}{Z_2^{1/3}} \frac{k/E_i}{E_i(1 - k/E_i)}\end{aligned}\quad (2.44)$$

This parameter results from dividing the Thomas–Fermi radius of the atom [15]

$$r_a = \frac{a_0}{Z_2^{1/3}} = \frac{\hbar}{\alpha mc Z_2^{1/3}}\quad (2.45)$$

by the maximum allowed value of  $\hbar/q$  [12]. The quantity  $a_0$  is the ground state radius of the hydrogen atom in the Bohr theory and

$$\alpha = e^2/\hbar c \approx 1/137\quad (2.46)$$

is the fine structure constant. The Bohr radius  $a_0$  is related to the classical radius of the electron by  $r_e = \alpha^2 a_0$ . The case of complete screening corresponds to  $\Gamma \approx 0$ . Figure 2.9a shows the region of allowed photon energies as a function of the incident electron energy. The contour with  $\Gamma = 0.1$  for lead is shown together with the region of complete screening.

Measurements of the angular distribution of bremsstrahlung photons agree with the predictions of the Bethe–Heitler calculations [16]. If the angles are measured with respect to the incident electron direction, the differential cross section is given approximately by

$$\frac{d\sigma}{(dp_f/p_f) d\Omega_f d\Omega_\gamma} = \frac{8Z_2^2\alpha^3}{\pi^2} \frac{p_f(p_i^2 + p_f^2)}{k p_i^4 \theta_i^2 \theta_\gamma^2 (\theta_f + \theta_\gamma)^2} \frac{r^2}{(1 + r^2)^2}\quad (2.47)$$

where i (f) refers to the incoming (outgoing) electron and  $r = Q_\perp/Q_\parallel$  is the ratio of the 3-momentum transfer to the nucleus perpendicular and parallel to the incident electron direction.

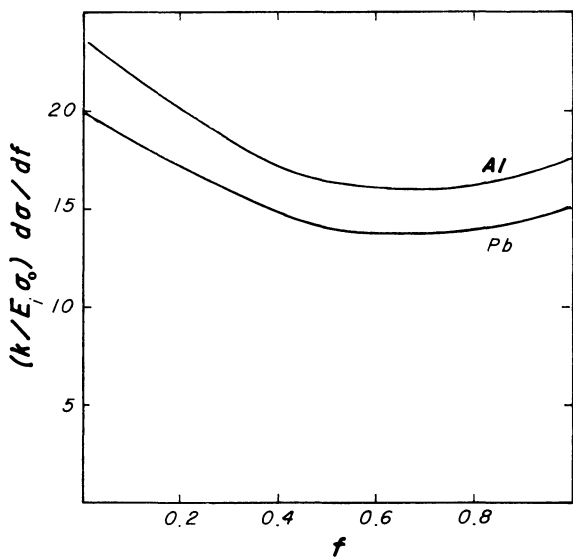
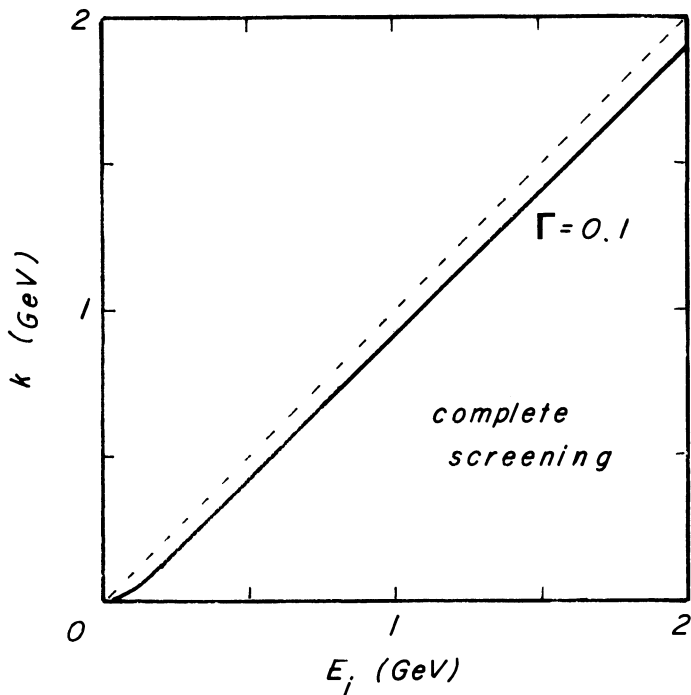
At high energy the mean angle of photon emission is

$$\bar{\theta}_\gamma \approx \frac{mc^2}{E}\quad (2.48)$$

independent of the photon energy. Thus, most of the radiation lies inside a narrow cone around the electron's momentum vector. The cone becomes more and more narrow as the energy is increased. Bremsstrahlung photons are in general polarized with the polarization vector normal to the plane formed by the photon and incident electron [3]. The photon polarization is influenced by the polarization of the incident electrons.

The cross section integrated over angles in the case of complete screen-

**Figure 2.9** (a) The kinematic region of complete screening for bremsstrahlung and the contour for lead with  $\Gamma = 0.1$ . (b) The complete screening bremsstrahlung cross sections for aluminum and lead versus the variable  $f = k/(E_i - mc^2)$ .



ing ( $\Gamma \ll 1$ ) is [12]

$$\frac{d\sigma}{dk} = \frac{4\sigma_0}{k} \left[ \left( 1 + w^2 - \frac{2}{3}w \right) \ln \frac{183}{Z_2^{1/3}} + \frac{w}{9} \right] \quad (2.49)$$

where  $w = E_f/E_i$  and  $E_i \gg mc^2$ , and

$$\sigma_0 = \alpha Z_2^2 r_e^2 \quad (2.50)$$

The contribution of the atomic electrons can be included by substituting  $Z_2^2 \rightarrow Z_2(Z_2 + 1)$ . Note that Eq. 2.49 only depends on the fractional energy  $w$  and not on  $E_i$  itself. It also depends on the material principally through the factor  $Z_2^2$  in  $\sigma_0$ .

Expressions for the cross section for the case  $\Gamma > 0$  have been defined using auxiliary functions and can be found in the literature [1, 12]. For  $\Gamma = 0.1$  the complete screening approximation in lead differs from the more accurate partial screening calculations by  $\sim 3\%$ . It can be seen that to this level of approximation and so long as  $E_i \gg mc^2$ , one may assume complete screening, except for the production of very energetic photons that carry off almost all of the electron's energy.

The factor  $k$  in the denominator of Eq. 2.49 implies that the cross section for low energy photon production increases without limit. Of course, this infrared divergence does not actually occur. These equations are not valid in the limit  $k \rightarrow 0$ .

For the purpose of illustrating the energy dependence of the bremsstrahlung cross sections, it is convenient to use as the independent variable

$$f = \frac{k}{E_i - mc^2}$$

which is the fraction of the incident kinetic energy of the electron given to the photon. Multiplying the cross section by  $k$  gives the photon intensity distribution. The complete screening cross sections for aluminum and lead are shown in Fig. 2.9b. For very energetic photon production (large  $f$ ) screening corrections are negligible. The most important feature of Fig. 2.9b is that the energy distribution does not fall off much faster than  $1/k$ . Hence there is a significant probability of obtaining a photon of any energy up to the maximum allowed. The deposited energy spectrum  $d\sigma/df$  is fairly uniform. The function plotted in Fig. 2.9b only changes a small amount for different elements. Hence the major material dependent factor is the  $Z^2$ , which comes from  $\sigma_0$ .

The energy loss due to radiation of an electron traversing some material is as follows:

$$\left. \frac{dE}{dx} \right|_{\text{rad}} = \int_0^{k_{\text{max}}} k n_a \frac{d\sigma}{dk} dk$$

where  $k_{\text{max}} = E_i - mc^2$  is the maximum allowed photon energy. It is convenient to separate out the incident energy and write the energy loss as

$$\left. \frac{dE}{dx} \right|_{\text{rad}} = n_a E_i \sigma_{\text{rad}} \quad (2.51)$$

where

$$\sigma_{\text{rad}} = \frac{1}{E_i} \int_0^{k_{\text{max}}} k \frac{d\sigma}{dk} dk$$

For the case of complete screening and  $E_i \gg mc^2/\alpha Z^{1/3}$

$$\sigma_{\text{rad}} = 4\sigma_0 [\ln(183Z_2^{-1/3}) + \frac{1}{18}] \quad (2.52)$$

Note that  $\sigma_{\text{rad}}$  in this case is independent of the electron's energy. Thus, according to Eq. 2.51 the energy loss due to radiation is proportional to  $E_i$ . The collision energy loss, on the other hand, increased like  $\ln E_i$ . In addition, the radiative energy loss is proportional to  $Z_2^2$ , whereas the collision loss was proportional to  $Z_2$ . If we rewrite Eq. 2.51 in the form  $dE/E = dx n_a \sigma_{\text{rad}}$ , we see that  $n_a \sigma_{\text{rad}}$  must be the inverse of some constant length  $L_R$ , where

$$L_R^{-1} = 4\sigma_0 n_a \ln(183Z_2^{-1/3}) \quad (2.53)$$

and we have neglected the small term  $\frac{1}{18}$  in Eq. 2.52. If we also neglect the collisional energy loss, we find that radiation losses cause the mean energy of the electron to decrease exponentially so long as the restrictions on Eq. 2.52 are satisfied.

Values of  $L_R$  for various materials are listed in Table 2.1. Radiation lengths for molecules can be determined from the atomic values by weighting the terms by the appropriate atomic weight [14]. It is often convenient to express lengths as a multiple of the radiation length in the material.

The ratio of the radiation energy loss to the collision energy loss is given approximately by [12]

$$\left. \frac{dE}{dx} \right|_{\text{rad}} / \left. \frac{dE}{dx} \right|_{\text{coll}} = \frac{Z_2 E_i}{1600 mc^2}$$

We see that at high incident electron energies, the energy loss is almost totally due to the production of radiation. The energy at which the loss due to radiation just equals the loss due to ionization is sometimes called the critical energy



$$E_{\text{crit}} = \frac{1600}{Z_2} mc^2 \quad (2.54)$$

Another process by which fast moving charged particles can lose energy is through direct pair production [15]. The electromagnetic field of the charged particle may be considered as a flux of virtual photons. In the Coulomb field of the nucleus or an electron the virtual photons can decay into an electron and positron, just as real photons do in the process of pair production.

We have seen that the dominant source of energy loss for high energy electrons is through bremsstrahlung. Figure 2.9b showed the energy distribution of the photons as a function of the fraction of the initial kinetic energy given to the photon. We saw that there was a substantial probability that the emitted photon will carry off a large fraction of the electron's energy. Thus, we expect that the distribution of electron energy losses will be quite wide compared to that of a heavy charged particle. The Landau theory discussed in Section 2.3 is only applicable to low energy electrons, whose energy losses are dominated by collision processes. At high energies the probability due to bremsstrahlung that the energy of an electron will decrease by the factor  $e^{-\zeta}$  while traversing a thickness  $x$  of material is [15]

$$w(x, \zeta) = \frac{e^{-\zeta} \zeta^{bx-1}}{\Gamma(bx)} \quad (2.55)$$

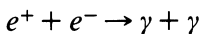
where

$$b \sim 21 n_a \sigma_0$$

and  $\Gamma$  is the gamma function. This relation is only valid for small thicknesses of low  $Z$  material. Otherwise, the electron has a large probability of initiating an electromagnetic shower (see Section 11.1).

### 2.4.3 Positron annihilation

The ultimate fate of most positrons in matter is annihilation with an electron into photons. The most likely process is



Annihilation into a single photon is possible if the electron is bound to a nucleus, but the cross section for this process is at most 20% of that for two photons [15]. The two-photon annihilation cross section for a positron with LAB energy  $E_+$  is given by

$$\sigma_{\text{ann}} = \pi r_e^2 \frac{1}{\gamma + 1} \left[ \frac{\gamma^2 + 4\gamma + 1}{\gamma^2 - 1} \ln(\gamma + \sqrt{\gamma^2 - 1}) - \frac{\gamma + 3}{\sqrt{\gamma^2 - 1}} \right] \quad (2.56)$$

where

$$\gamma = E_+/mc^2$$

This cross section peaks near  $\gamma = 1$ . Thus, it is most likely that a high energy positron will lose energy by collision and radiation until the velocity becomes small, at which point it will annihilate into photons.

The electron and the positron can also form a temporary bound state called positronium. This system is analogous to the hydrogen atom, although the energy level spacing is reduced by a factor of 2 due to the reduced mass of the electron – positron system. Annihilation occurs when there is an overlap between the electron and positron wavefunctions and is most likely in the *S* state. The two particles can form both singlet (spins antiparallel) and triplet (spins parallel) states. The most common decay is the singlet state decay at rest into two collinear 0.511-MeV photons, which occurs with a mean lifetime of  $\sim 10^{-10}$  sec. The triplet state decays into three photons with a mean lifetime of  $\sim 10^{-7}$  sec.

## 2.5 Interactions of photons

We have seen that the collisional interactions of heavy charged particles tend to be small perturbations that, apart from removing a small amount of energy and causing a small change in the particle's trajectory, leave the particle basically undisturbed. Thus, the number of particles in a beam remains roughly constant until the velocity has been reduced to a small value. Photon interactions are different since in general there is a large probability that an interacting photon will be removed from the beam.

Consider a collimated, monoenergetic beam of  $N$  photons. The number removed from the beam while crossing a thickness  $dx$  of material is

$$dN = -\mu N dx \quad (2.57)$$

The constant of proportionality  $\mu$  is known as the linear attenuation coefficient and is related to the probability that a photon will be scattered or absorbed in the material [17]. As a consequence, the intensity of the original photons will decrease exponentially with depth in matter.

There are three major electromagnetic processes by which photons interact with matter:

1. photoelectric effect,
2. Compton effect, and
3. pair production.

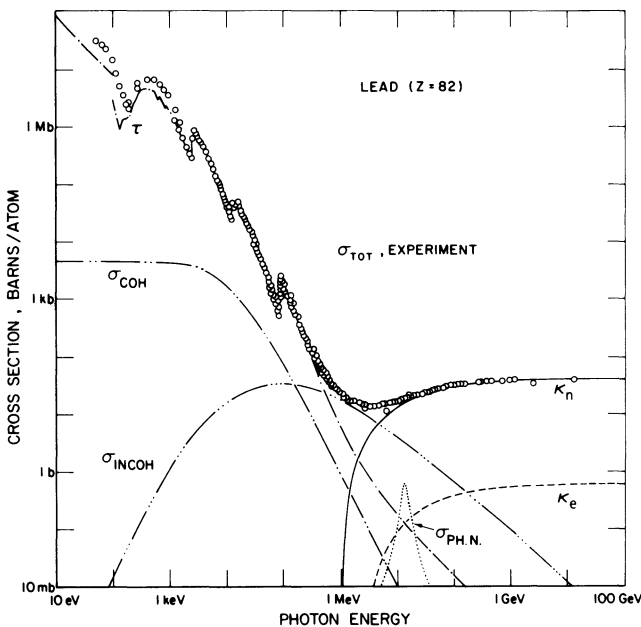
Figure 2.10 shows the contributions of these three processes to the total photon interaction cross section for lead. For photon energies below 500

keV the interactions are almost totally due to the photoelectric effect, while for photon energies above 50 MeV they are primarily due to pair production off the nucleus. The Compton effect plays an important role in the intermediate energy range. Two other effects indicated in Fig. 2.10 are coherent (Rayleigh) scattering and photonuclear absorption. Rayleigh scattering is a process in which photons scatter from the atomic electrons without exciting or ionizing the atom. Photonuclear absorption is actually a nuclear interaction where the photon is absorbed by the nucleus. It is most important in the region of the “giant resonance” (10–25 MeV) and is frequently accompanied by the emission of a neutron.

### 2.5.1 Photoelectric effect

The photoelectric effect can be considered to be an interaction between the photon and the atom as a whole. Incident photons whose energy  $k$  exceeds the binding energy  $E_b$  of an electron in the atom may be absorbed, and an atomic electron ejected with kinetic energy  $T = k - E_b$ . The photoelectron is emitted near  $90^\circ$  from the incident photon direction

**Figure 2.10** Contributions to the photon interaction cross section in lead.  $\tau$ , photoelectric effect;  $\sigma_{\text{COH}}$ , Rayleigh scattering;  $\sigma_{\text{INCOH}}$ , Compton scattering;  $\sigma_{\text{PH,N}}$ , photonuclear absorption;  $K_n$ , pair production off the nucleus;  $K_e$ , pair production off atomic electrons. (J. Hubbell, H. Gimm, and I. Overbo, J. Phys. Chem. Ref. Data 9: 1023, 1980.)



for very low energy, unpolarized photons [15]. The emission angle becomes more and more forward as the photon energy increases. However, the directionality can be quickly randomized due to multiple scattering.

There are sharp discontinuities in the photoelectric spectrum corresponding to the binding energies of the atomic shells, the most prominent of which is due to the innermost, or  $K$ , shell. The cross section increases by a large factor when the photon energy exceeds the binding energy of electrons in the shell. The ejected photoelectron may be accompanied by fluorescence or additional (Auger) electrons. The photoelectric cross section at high energies falls roughly as  $Z^5/k$  and only plays a negligible role in high energy interactions.

### 2.5.2 Compton effect

The Compton effect involves the scattering of an incident photon with an atomic electron. Consider a photon with energy  $k_0$  scattering from an electron considered to be at rest and producing a scattered photon with energy  $k$  together with the recoiling electron, as shown in Fig. 2.11. The laws of conservation of energy and momentum require that

$$k_0 + mc^2 = k + T + mc^2$$

$$\mathbf{k}_0 = \mathbf{k} + \mathbf{p}$$

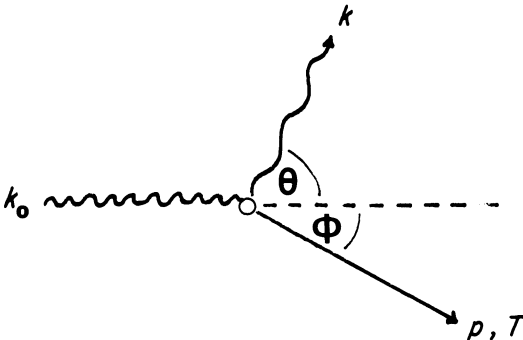
These equations can be solved in terms of the scattering angle  $\theta$  to obtain the frequency of the scattered photon [15],

$$\omega = \frac{\omega_0}{1 + \epsilon(1 - \cos \theta)} \quad (2.58)$$

the kinetic energy of the recoil electron,

$$T = mc^2 \frac{\epsilon^2(1 - \cos \theta)}{1 + \epsilon(1 - \cos \theta)} \quad (2.59)$$

**Figure 2.11** The Compton scattering process.



and the electron recoil angle

$$\cos \phi = (1 + \epsilon) \left[ \frac{1 - \cos \theta}{2 + \epsilon(\epsilon + 2)(1 - \cos \theta)} \right]^{1/2} \tag{2.60}$$

where

$$\epsilon = \hbar\omega_0/mc^2$$

We can express the difference in the wavelength of the incident and scattered photons as

$$\lambda - \lambda_0 = h/mc(1 - \cos \theta) \tag{2.61}$$

The scattered photon has a longer wavelength than the incident one. The quantity  $h/mc$  is referred to as the Compton wavelength of the electron.

The quantum mechanical derivation of the cross section for Compton scattering was performed by Klein and Nishima. The differential cross section averaged over the polarization of the incident photon is [12]

$$\frac{d\sigma}{d\Omega} = \frac{1}{2} r_e^2 \left( \frac{h\omega}{h\omega_0} \right)^2 \left( \frac{h\omega_0}{h\omega} + \frac{h\omega}{h\omega_0} - \sin^2 \theta \right) \tag{2.62}$$

If we use Eq. 2.58 to eliminate  $\omega$  from this equation, we obtain the angular distribution

$$\frac{d\sigma}{d\Omega} = \frac{1}{2} r_e^2 \frac{(1 + \cos^2 \theta)}{[1 + \epsilon(1 - \cos \theta)]^2} \left\{ 1 + \frac{\epsilon^2(1 - \cos \theta)^2}{(1 + \cos^2 \theta)[1 + \epsilon(1 - \cos \theta)]} \right\} \tag{2.63}$$

This distribution is shown as a function of energy and scattering angle in Fig. 2.12. The angular distribution of scattered radiation from classical electrodynamics is [2]

$$I = I_0(1 + \cos^2 \theta)$$

independent of frequency. The quantum results should approach the classical one as  $\hbar \rightarrow 0$  and thus as  $\epsilon \rightarrow 0$ . At high energies the scattered photons are produced mainly in the forward direction. The scattered photons may also be polarized.

The energy distribution may be obtained by substituting for  $\theta$  in Eq. 2.62. The result is [12]

$$\frac{d\sigma}{d(h\omega)} = \frac{\pi r_e^2}{\epsilon h\omega} \left[ 1 + \left( \frac{h\omega}{h\omega_0} \right)^2 - \frac{2(\epsilon + 1)}{\epsilon^2} + \frac{1 + 2\epsilon}{\epsilon^2} \frac{h\omega}{h\omega_0} + \frac{1}{\epsilon^2} \frac{h\omega_0}{h\omega} \right] \tag{2.64}$$

where the scattered photon energy must satisfy the inequality

$$\frac{1}{1 + 2\epsilon} \leq \frac{h\omega}{h\omega_0} \leq 1$$

For small  $\epsilon$  there is only a small spread of scattered photon energies, close to the incident photon energy. For higher energies the number of low energy scattered photons increases and the distribution becomes very broad.

The total cross section for photon scattering from classical electrodynamics is the Thomson cross section [3]

$$\sigma_{\text{Th}} = \frac{8}{3}\pi r_e^2 \approx 0.67 \times 10^{-24} \text{ cm}^2$$

The quantum mechanical result is obtained by integrating Eq. 2.63 over all angles giving [12]

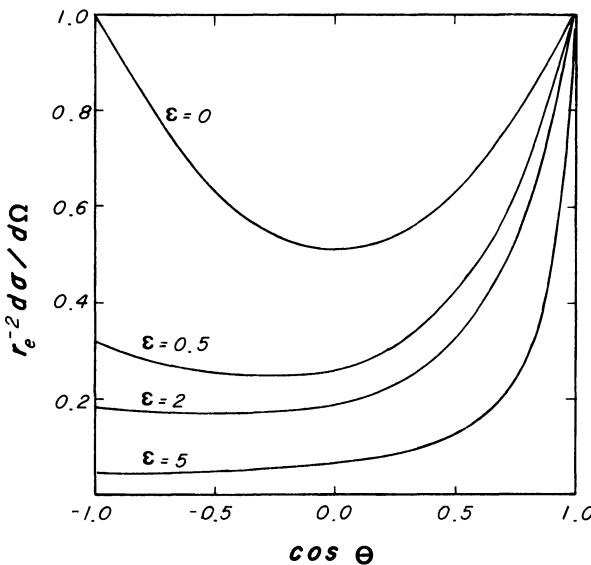
$$\sigma_{\text{Comp}} = \sigma_{\text{Th}} \frac{3}{8\epsilon} \left\{ \left[ 1 - \frac{2(\epsilon + 1)}{\epsilon^2} \right] \ln(2\epsilon + 1) + \frac{1}{2} + \frac{4}{\epsilon} - \frac{1}{2(2\epsilon + 1)^2} \right\} \quad (2.65)$$

At high energy the cross section is given approximately by

$$\sigma_{\text{Comp}} \approx \sigma_{\text{Th}} \frac{3}{8\epsilon} \left( \ln 2\epsilon + \frac{1}{2} \right)$$

Thus, at high energy the Compton scattering per atom will fall off roughly like  $Z_2/h\omega_0$ .

**Figure 2.12** The angular distribution for Compton scattering. The parameter  $\epsilon = h\omega_0/mc^2$ .



2.5.3 Pair production

The third interaction of photons in matter and the most important at high energies is pair production. The intense electric field near the nucleus can cause the photon to decay into an electron and a positron. The threshold energy for this process is  $2mc^2$ . The nucleus must be there to satisfy conservation of momentum, but it acquires very little recoil energy. Pair production may also take place near an atomic electron. The threshold in this case is  $4mc^2$ , and the recoil electron acquires significant kinetic energy. In a track sensitive detector this would appear as a triplet of tracks.

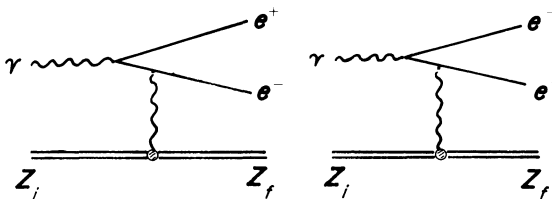
The bremsstrahlung and pair creation processes are intimately related in QED. Examination of the Feynman diagrams in Figs. 2.8 and 2.13 shows that the effects differ only in the directions of the incident and outgoing particles. Both processes proceed to lowest order through the exchange of a single virtual photon. As a consequence, both effects are most important when the momentum transfer is small.

Bethe and Heitler made a quantum mechanical calculation of the cross section for pair creation in the Born approximation. The matrix elements can be determined from those used in the bremsstrahlung calculation with some simple substitutions. This comes about in the Dirac theory since one can regard the inverse of pair production as a bremsstrahlung process in which a positive energy electron emits a photon and falls into a negative energy state [12].

Screening of the nucleus by the atomic electrons is again an important effect. Let the incident photon have energy  $k$  and the created electron (positron) have energy  $E_-$  ( $E_+$ ) so that  $k = E_+ + E_-$ . The screening is measured using the parameter

$$\begin{aligned} \Gamma' &= \frac{100mc^2}{Z_2^{1/3}} \frac{k}{E_+ E_-} \\ &= \frac{100mc^2}{Z_2^{1/3}} \frac{1}{kw_+(1-w_+)} \end{aligned} \tag{2.66}$$

Figure 2.13 Lowest-order Feynman diagrams for pair production.



where we have used the energy ratios  $w_{\pm} = E_{\pm}/k$ . Note that the screening parameter is symmetric in  $w_+$  and  $w_- = 1 - w_+$  and decreases in general with increasing  $k$ . For a given value of  $k$  the screening parameter is smallest for symmetric pairs, the limit where  $\Gamma' \sim 0$  corresponding to complete screening. Figure 2.14a shows the contour with  $\Gamma' = 0.1$  for lead and the region of complete screening on a graph of  $E_+$  versus  $k$ .

The differential cross section for the production of a positron with energy between  $E_+$  and  $E_+ + dE_+$  and an electron of energy  $E_- = k - E_+$  from a photon with energy  $k$  in the limit of complete screening is [12]

$$\frac{d\sigma}{dE_+} = \frac{4\sigma_0}{k} \left[ \left( w_+^2 + w_-^2 + \frac{2}{3} w_+ w_- \right) \ln \left( \frac{183}{Z_1^{1/3}} \right) - \frac{1}{9} w_+ w_- \right] \quad (2.67)$$

where  $\sigma_0$  was given by Eq. 2.50. Note that Eq. 2.67 is symmetric between electron and positron energies. Actually at very low energies where the Born approximation is no longer valid, nuclear repulsion tends to make the positrons more energetic than the electrons. The cross section for the case  $\Gamma' > 0$  can be expressed in terms of the same auxiliary functions used for bremsstrahlung [12]. The corrections to the complete screening approximation for lead when  $\Gamma' = 0.1$  is  $\sim 3\%$ .

The pair production cross section is conveniently expressed as a function of the variable

$$g = \frac{E_+ - mc^2}{k - 2mc^2}$$

which is the fraction of the total available kinetic energy taken by the positron. Figure 2.14b shows the complete screening cross sections for lead and aluminum normalized to  $\sigma_0$  and plotted as a function of the variable  $g$ . The cross sections are fairly uniform, indicating that positrons are likely to be produced with any allowed energy. Thus, in general, the electron and the positron in the pair do not have the same energy. Since the plotted functions vary little for different elements, the major material dependence is again the  $Z_1^2$  factor that comes from  $\sigma_0$ . When  $g = 0$  or  $g = 1$ , the complete screening approximation is no longer valid. The correct theory causes the cross section to fall off rapidly for these cases.

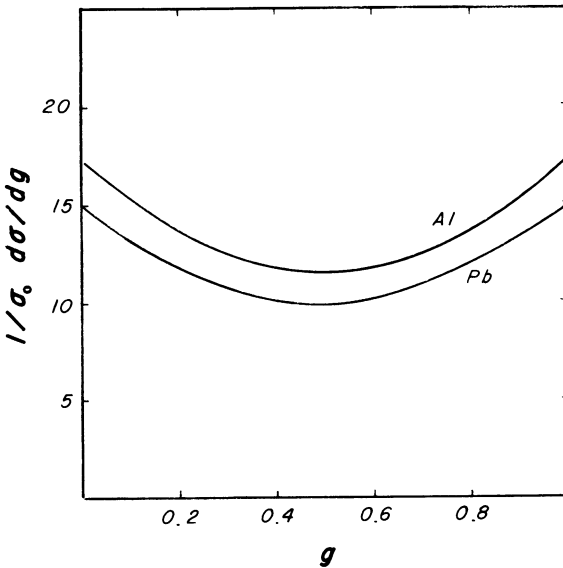
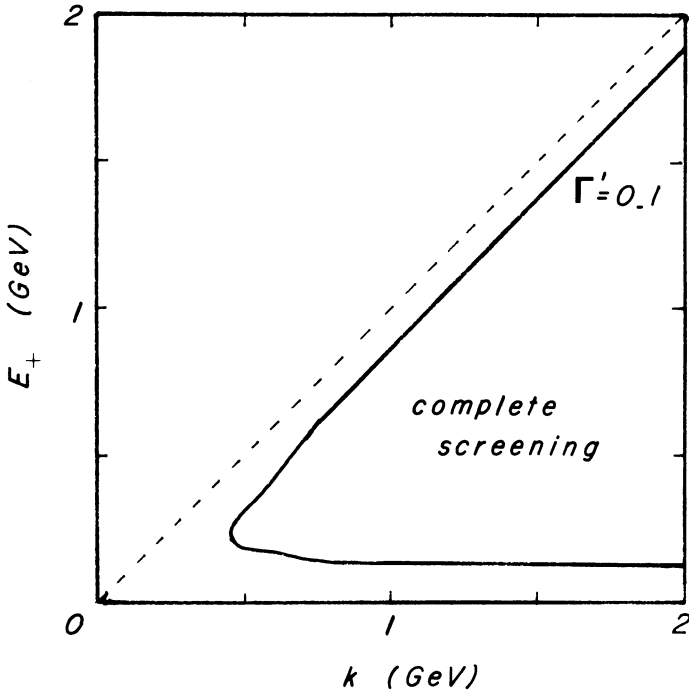
At high energy the electron and positron tend to be produced at small angles with respect to the incident photon direction. The mean production angle of an electron or positron with energy  $E$  is approximately [12]

$$\theta = \frac{mc^2}{E} \quad (2.68)$$

The total pair production cross section is obtained by integrating Eq.



**Figure 2.14** (a) The kinematic region of complete screening for pair production and the contour for lead with  $\Gamma' = 0.1$ . (b) Complete screening pair production cross sections for aluminum and lead versus the variable  $g = (E_+ - mc^2)/(k - 2mc^2)$ .



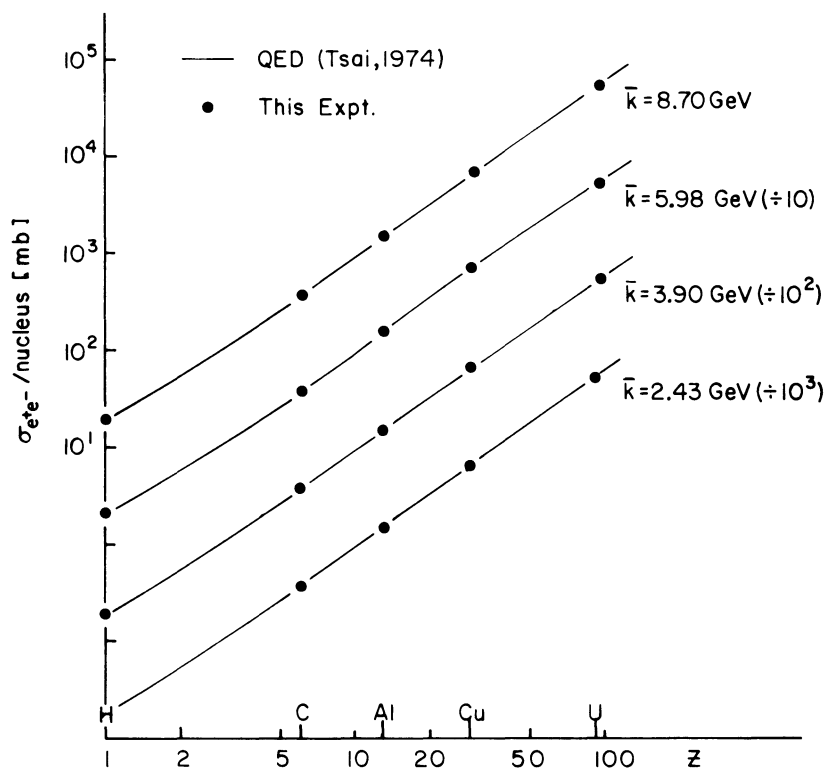
2.67 over all possible positron energies. The total cross section increases rapidly as the photon energy increases, approaching the asymptotic value

$$\sigma_{\text{pair}} = 4\sigma_0 \left[ \frac{7}{9} \ln(183Z_2^{-1/3}) - \frac{1}{34} \right] \quad (2.69)$$

for  $k \gg 137mc^2Z^{-1/3}$ . Note that the cross section is approximately proportional to  $Z^2$  and is independent of the incident photon energy. If we compare Eq. 2.69 with Eq. 2.52, we see that the cross section for pair production is roughly seven-ninths that for bremsstrahlung.

Total cross sections for pair production off of the nucleus and atomic electrons in lead were shown in Fig. 2.10. Pair production off the nucleus contributes over 95% of the photon total cross section at 60 MeV. The majority of the remaining 5% is due to Compton scattering. The assumptions used in the Born approximation break down for high  $Z$  elements. The actual cross section for lead is about 10% smaller than the calculated one [12].

**Figure 2.15** Measurements of the pair production cross section as a function of the average photon energy  $\bar{k}$  and the atomic number  $Z$  of the absorber. Solid lines are QED calculations. (J. Eickmeyer et al., Phys. Rev. D 21: 3001, 1980.)



A summary of the results of QED calculations of pair production is contained in the review of Tsai [14]. Figure 2.15 presents a comparison of these calculations for the total cross section with experimental measurements of high energy pair production by Eickmeyer et al. [18]. The calculations are in excellent agreement with the measurements for all elements and photon energies over the range 2.4–8.7 GeV.

In a homogeneous medium the intensity of a beam of collimated, monoenergetic photons decreases exponentially

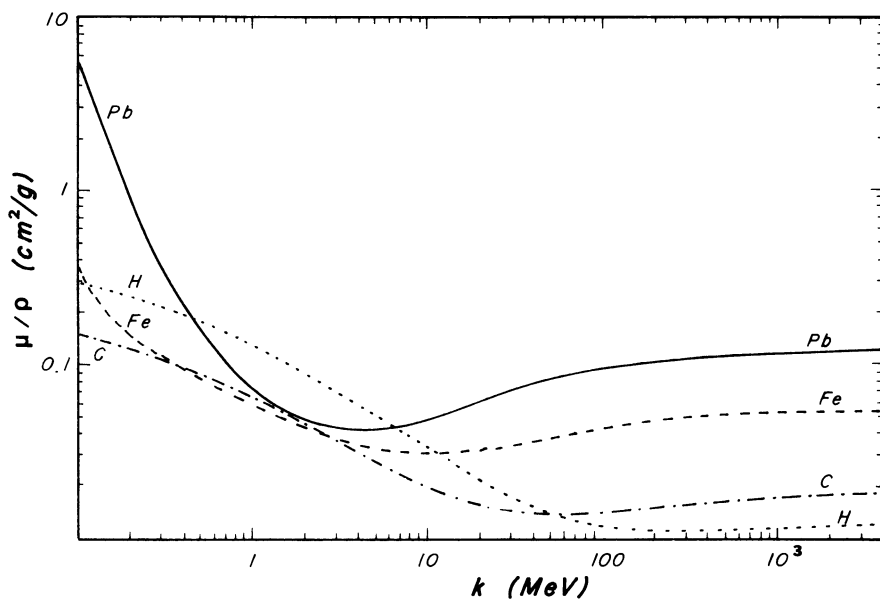
$$I(x) = I_0 \exp(-\mu x)$$

where  $\mu$  is the linear attenuation coefficient. The coefficient  $\mu$  is frequently divided by the density to obtain the mass attenuation coefficient  $\mu/\rho$ , which has the dimensions  $\text{cm}^2/\text{g}$ . The mass attenuation coefficient is related to the total photon interaction cross section  $\sigma_{\text{tot}}$  by

$$\begin{aligned} \frac{\mu}{\rho} &= \frac{N_A}{A} \sigma_{\text{tot}} \\ &\approx \frac{N_A}{A} (\sigma_{\text{pE}} + Z\sigma_{\text{Comp}} + \sigma_{\text{pair}}) \end{aligned} \quad (2.70)$$

where  $A$  is the atomic weight of the material. Figure 2.16 shows the mass

**Figure 2.16** Photon mass attenuation coefficients for H, C, Fe, and Pb as a function of photon energy. (Data from J. Hubbell, H. Gimm, and I. Overbo, *J. Phys. Chem. Ref. Data* 9: 1023, 1980; J. Hubbell, National Bureau of Standards report NSRDS-NBS 29, 1969.)



attenuation coefficients for a number of materials as a function of the incident photon energy.

## 2.6 Elastic scattering

We have seen that the dominant source of energy loss for heavy charged particles is the inelastic excitation and ionization of atomic electrons. The energy loss resulted from the Coulomb interaction between the incident particles and the atomic electrons. So far we have considered the particle's trajectory to be a straight line through the absorber. However, the force on the incident particle due to the charged particles in the absorber can also introduce small deflections in the trajectory.

Consider a charged particle traversing a thickness of material. We saw in Section 2.1 that the Coulomb field of the incident particle gives the charged particles in the medium a momentum perpendicular to the original direction of

$$p_{\perp} = \frac{2Z_1 Z_2 e^2}{bv}$$

The incident particle receives an oppositely directed momentum of the same magnitude. It will therefore be deflected through a small angle

$$\theta \simeq \frac{p_{\perp}}{p} = \frac{2Z_1 Z_2 e^2}{bvp} \quad (2.71)$$

The differential cross section for scattering with an impact parameter between  $b$  and  $b + db$  is  $2\pi b db$ . Using Eq. 2.71, we can relate this to the cross section for scattering between  $\theta$  and  $\theta + d\theta$ ,

$$d\sigma = 2\pi \left( \frac{2Z_1 Z_2 e^2}{pv} \right)^2 \frac{d\theta}{\theta^3}$$

In the small angle approximation the solid angle  $d\Omega \simeq 2\pi\theta d\theta$ . It follows that the small angle form of the elastic differential cross section can be written in the form

$$\frac{d\sigma}{d\Omega} = 4Z_1^2 Z_2^2 r_e^2 \left( \frac{mc}{\beta p} \right)^2 \frac{1}{\theta^4} \quad (2.72)$$

The  $\theta^{-4}$  dependence of the cross section shows that a particle is much more likely to undergo a small angle scatter than a large one.

The exact form of the scattering differential cross section for a Coulomb potential in both classical and quantum mechanics is the Rutherford scattering formula

$$\frac{d\sigma}{d\Omega_{\mathbf{R}}} = \frac{1}{4} Z_1^2 Z_2^2 r_e^2 \left( \frac{mc}{\beta p} \right)^2 \frac{1}{\sin^4(\theta/2)} \quad (2.73)$$

This cross section is valid for a spin 0 incident particle. The cross section for the interaction of a spin  $\frac{1}{2}$  incident particle in the Coulomb field of a nucleus is the Mott cross section, given by [1]

$$\frac{d\sigma}{d\Omega_M} = \frac{d\sigma}{d\Omega_R} \left( 1 - \beta^2 \sin^2 \frac{\theta}{2} \right) \quad (2.74)$$

We see that the additional term, which arises from the use of spinor wavefunctions, is only important for large  $\beta$  and large  $\theta$ . For small angle scattering the Mott cross section reduces to the Rutherford case.

The elastic differential cross section for the scattering of two relativistic electrons is known as the Moller cross section and is given in the CM frame by [19]

$$\frac{d\sigma}{d\Omega} = \frac{\alpha^2}{4s} \left[ \frac{10 + 4x + 2x^2}{(1-x)^2} + \frac{10 - 4x + 2x^2}{(1+x)^2} + \frac{16}{(1-x)(1+x)} \right] \quad (2.75)$$

where  $x = \cos \theta^*$  and  $s$  is the total CM energy squared. The corresponding cross section for positrons and electrons was derived by Bhabha. A QED calculation of the relativistic cross section gives

$$\frac{d\sigma}{d\Omega} = \frac{\alpha^2}{4s} \left[ \frac{10 + 4x + 2x^2}{(1-x)^2} - \frac{2(1+x)^2}{1-x} + (1+x^2) \right] \quad (2.76)$$

The excellent agreement of the calculation with measurements [20] of the cross section between 14 and 34 GeV is shown in Fig. 2.17.

The Rutherford scattering cross section is not valid at very small or very large angles. For very small angles, which correspond to very large impact parameters, the Coulomb potential of the nucleus is screened by the presence of the atomic electrons. The effective potential drops sharply for separation distances that exceed the Thomas–Fermi radius of the atom given in Eq. 2.45. This has the effect of modifying the small angle Rutherford cross section to [2]

$$\frac{d\sigma}{d\Omega} = 4Z_1^2 Z_2^2 r_e^2 \left( \frac{mc}{\beta p} \right)^2 \frac{1}{(\theta^2 + \theta_{\min}^2)^2} \quad (2.77)$$

The cross section for scattering at angles less than some angle  $\theta_{\min}$  will be very small. The form of Eq. 2.77 shows that instead of diverging at  $\theta = 0$  the cross section levels off to a constant value.

We can estimate  $\theta_{\min}$  classically using Eq. 2.71 with  $b$  evaluated at the atomic radius  $r_a$

$$\theta'_{\min} \approx 2Z_1 Z_2^{4/3} \frac{mc^2}{pv} \left( \frac{r_e}{a_0} \right) \quad (2.78)$$

A quantum mechanical limit on  $\theta$  arises since the incident trajectory must be localized to within  $\Delta x \sim r_a$  to obtain a reasonable probability of scat-

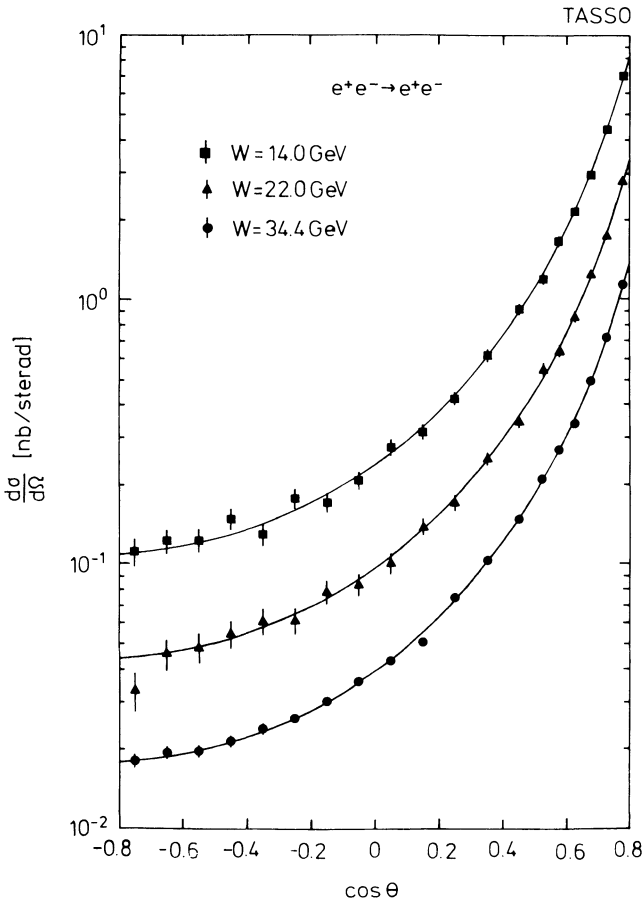
tering. Then, by the uncertainty principle, the incident momentum is uncertain by an amount  $\Delta p \sim \hbar/r_a$  and the scattering angle by  $\Delta\theta \sim \hbar/pr_a$ . Scattering for angles smaller than  $\Delta\theta$  is smeared, causing the cross section to flatten out. Using Eq. 2.45 for the atomic radius, we find

$$\theta_{\min} = \alpha Z^{1/3} \frac{mc}{p} \tag{2.79}$$

In general, the more restrictive of the two limits should be used.

The Rutherford scattering law also breaks down when the particle's wavelength  $\lambda$  becomes comparable with the size  $r_n$  of the nucleus. In

**Figure 2.17** Angular distributions for Bhabha scattering. Solid lines are results of QED calculations. (R. Brandelik et al., Phys. Lett. 117B: 365, 1982.)



analogy with the first minimum of a diffraction pattern from an object of size  $r_n$ , the scattering is predominantly confined to angles smaller than

$$\theta_{\max} \approx \frac{\lambda}{r_n} \approx \frac{\hbar}{pr_n}$$

Using the simple relation [1, 2]

$$r_n \approx \frac{1}{2} r_e A^{1/3} \quad (2.80)$$

we find that

$$\theta_{\max} \approx \frac{2A^{-1/3}}{\alpha} \frac{mc}{p} \quad (2.81)$$

Other corrections that are sometimes important include the mass of the target and particle identity.

The total elastic scattering cross section can be estimated by integrating Eq. 2.72 from  $\theta_{\min}$  to  $\theta_{\max}$ ,

$$\begin{aligned} \sigma &= \int \frac{d\sigma}{d\Omega} \sin \theta \, d\theta \, d\phi \\ &\approx \pi r_e^2 4 \left( \frac{Z_1 Z_2^{2/3}}{\alpha \beta} \right)^2 \end{aligned} \quad (2.82)$$

Note that the total elastic cross section falls off like  $\beta^{-2}$ .

## 2.7 Multiple scattering

We have seen in the previous section that there is a significant probability that a charged particle will undergo a Coulomb scattering collision while traversing a block of matter. Suppose that downstream of the block we observe how many particles are traveling at an angle  $\theta$  with respect to the incident beam direction. Figure 2.18 shows the trajectories of two particles. The first particle only makes a single scatter at the angle  $\theta$ . On the other hand, since the cross section for Rutherford scattering grows rapidly for decreasing scattering angles, it is also possible for a particle to leave the block at the angle  $\theta$  after making a large number of small angle collisions. This latter case is referred to as multiple scattering. In a single event one cannot tell whether a particle observed at some angle has had a single scatter or has undergone multiple scattering. What one can do instead is to determine distribution functions for various processes, so that the probability of a given process resulting in a particle at the angle  $\theta$  can be calculated.

We have seen in Eq. 2.72 that the Coulomb scattering cross section is proportional to the squares of the incident particle and target charges. To

first order the probability for scattering due to the nucleus goes like  $Z_2^2$ , while the contribution of the  $Z_2$  atomic electrons goes like  $Z_2$ . Thus, except for the lightest elements, multiple scattering is dominated by Coulomb scattering off the nuclei.

Since each individual small angle scatter is a random process, we expect the mean scattering angle of a beam of particles with respect to the incident direction to be zero. On the other hand, the rms scattering angle will in general be nonzero. The expectation value of  $\theta^2$  due to multiple scattering of a particle while crossing a length  $L$  of the material is

$$\theta_s^2 = Ln_a \int \theta^2 \frac{d\sigma}{d\Omega} d\Omega$$

where we assume the particle's velocity is not appreciably reduced while crossing the material. Using the small angle Rutherford cross section (Eq. 2.72), we obtain the variance of the cumulative angle distribution

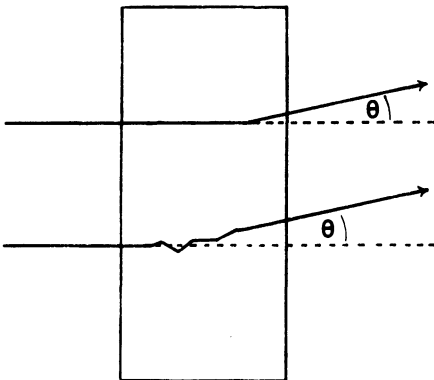
$$\theta_s^2 = 8\pi Ln_a r_e^2 Z_1^2 Z_2^2 \left(\frac{mc}{\beta p}\right)^2 \ln \frac{2}{\alpha^2 A^{1/3} Z_2^{1/3}} \tag{2.83}$$

where we have used Eqs. 2.79 and 2.81 for  $\theta_{\min}$  and  $\theta_{\max}$ . If we take  $A \approx 2Z$ , the logarithm factor can be written in the form  $2 \ln(173 Z_2^{-1/3})$ . This logarithmic dependence is similar to that encountered in the definition of the radiation length  $L_R$  in Eq. 2.53. Thus, rewriting Eq. 2.83 in terms of  $L_R$ , we get

$$\theta_s^2 = \frac{4\pi}{\alpha} Z_1^2 \frac{m^2 c^2}{\beta^2 p^2} \frac{L}{L_R}$$

Note that the expression of the multiple scattering angle in terms of a radiation length is just a convenience based on the fact that both quanti-

Figure 2.18 Scattering in a thick material.





ties have a similar dependence on the properties of the material. Multiple scattering is not a radiation process. Now combining some of the factors into the energy

$$E_s = \sqrt{4\pi/\alpha} mc^2 = 21.2 \text{ MeV} \tag{2.84}$$

we obtain the Rossi–Greisen equation for the rms scattering angle

$$\theta_s = \frac{E_s}{pv} Z_1 \sqrt{L/L_R} \tag{2.85}$$

This equation is only accurate if the particle traverses many radiation lengths of the material. Otherwise it tends to overestimate the amount of scattering.

Highland [21] has given a more accurate form of Eq. 2.85. He used the Moliere theory described below to investigate the dependence of  $E_s$  on  $Z$  and  $L$ . This leads to an empirical formula for  $\theta_e$ , the space angle for which the distribution drops to  $1/e$  of its peak value, of

$$\theta_e = \frac{17.5 \text{ MeV}}{pv} Z_1 \sqrt{\frac{L}{L_R}} \left[ 1 + 0.125 \log_{10} \left( \frac{10L}{L_R} \right) \right] \tag{2.86}$$

It is sometimes convenient to consider the projection of the scattering angle on a plane. Define the  $z$  axis of a right-handed coordinate system to be along the direction of motion of the incident particle as shown in Fig. 2.19. If  $\theta$  is the space angle of the scattered particle and  $\theta_x$  and  $\theta_y$  are the projections of the space angle onto the  $xz$  and  $yz$  planes, respectively, then

$$\cos \theta = (1 + \tan^2 \theta_x + \tan^2 \theta_y)^{-1/2}$$

Expanding for small  $\theta$ , we find  $\theta^2 \approx \theta_x^2 + \theta_y^2$ , so that on the average the angle projected onto a fixed plane is

$$\langle \theta_{pr}^2 \rangle = \frac{1}{2} \langle \theta^2 \rangle \tag{2.87}$$

Up to this point we have only been concerned with the rms or  $1/e$  values of the scattering angle. Another important question is the distribution of scattering angles. Let  $\psi_{ms}(\theta, x) \theta d\theta$  be the probability that a particle will emerge at an angle between  $\theta$  and  $\theta + d\theta$  with respect to the incident direction after traversing a finite thickness  $x$  of material. The distribution function is governed by a transport equation analogous to Eq. 2.30

$$\frac{\partial \psi_{ms}}{\partial x}(\theta, x) = \int \psi_{ms}(\theta - \zeta, x) n_a \frac{d\sigma}{d\Omega}(\zeta) \zeta d\zeta - \psi_{ms}(\theta, x) \int n_a \frac{d\sigma}{d\Omega}(\zeta) \zeta d\zeta \tag{2.88}$$

where we assume that the distribution is independent of the azimuthal scattering angle  $\phi$ .

Moliere has obtained a solution of this equation that, if we take  $d\sigma/d\Omega$

to be the small angle Rutherford cross section, becomes [22, 23]

$$\psi_{ms}(\theta, x) = \frac{1}{\theta_c^2} \int_0^\infty y dy J_0\left(\frac{\theta y}{\theta_c}\right) \exp\left[\frac{y^2}{4}\left(-b + \ln \frac{y^2}{4}\right)\right] \quad (2.89)$$

where  $J_0$  is a Bessel function and  $\theta_c$  is a characteristic angle given by

$$\theta_c^2 = \frac{4\pi n_a e^4 Z_1^2 Z_2 (Z_2 + 1)x}{(pv)^2} \quad (2.90)$$

The angle  $\theta_c$  contains the dependence of  $\psi_{ms}$  on the macroscopic properties of the scattering medium. Note that  $\theta_c^2$  grows linearly with  $x$ . The quantity  $b$  is defined as

$$b = \ln(\theta_c/\theta_a)^2 + 1 - 2C_E \quad (2.91)$$

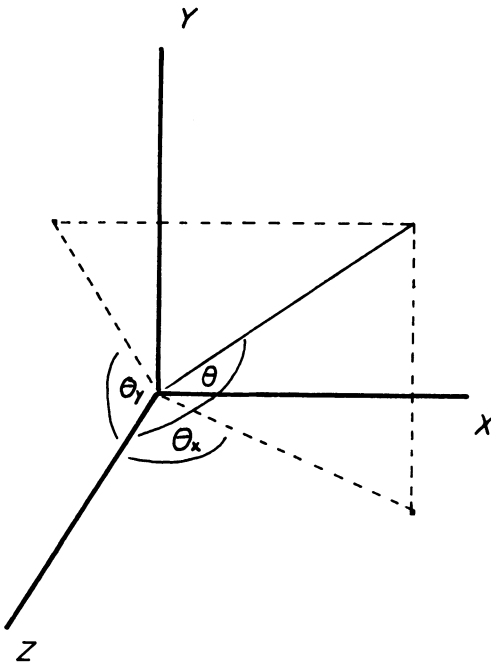
where  $C_E$  is Euler's constant. The dependence of the scattering on the screening angle  $\theta_a$  is given by

$$\theta_a^2 \approx \theta_0^2 \left[ 1.13 + 3.76 \left( \frac{Z_1 Z_2 e^2}{\hbar v} \right)^2 \right] \quad (2.92)$$

where  $\theta_0$  is approximately the minimum scattering angle given by Eq. 2.79,

$$\theta_0 \approx 1.13\theta_{min} \quad (2.93)$$

Figure 2.19 The projected scattering angles.



The Moliere theory should be valid when  $\theta_c \gg \theta_0$ . The scattering angle distribution approaches the Rutherford single scattering distribution for large angles.

The mean number of collisions between an incident particle and the target atoms in the thickness  $x$  can be found by dividing the target length by the interaction mean free path

$$N_{\text{coll}} = x/\lambda_1 = xn_a\sigma \quad (2.94)$$

If we use Eq. 2.82 for the total Coulomb scattering cross section, we find that

$$N_{\text{coll}} = 4xn_a\pi r_e^2 \left( \frac{Z_1 Z_2^{2/3}}{\alpha\beta} \right)^2 \quad (2.95)$$

When  $N_{\text{coll}} \geq 1000$ , the distribution is approximately Gaussian for small scattering angles.

Scattering angle distributions of 15.7 MeV electrons from gold foils are in excellent agreement with the predictions of the Moliere theory [24]. The small angle region is approximately Gaussian, and the tails fit nicely to the large angle, single scattering distributions. At high energies Shen et al. [25] have measured the small angle scattering distributions for  $\pi^\pm$ ,  $K^\pm$ , and  $p^\pm$  incident on H, Be, C, Al, Cu, Sn, and Pb targets. In each case the incident particle traversed about 0.1 radiation length of material. Figure 2.20 shows typical  $\theta^2$  distributions for hydrogen and lead. The experimental results for  $\theta_c$ , the angle at which the distribution drops to  $1/e$  of the peak value, agreed with the predictions of the Moliere theory. There was no statistically significant dependence on the type of projectile. The result for  $\theta_c$  from Eq. 2.86 was found to give results  $\sim 3\%$  larger than experiment for  $Z \geq 6$ . For  $Z < 6$  the error increased, reaching  $\sim 10\%$  for hydrogen.

The angular spread arising from multiple scattering also introduces a lateral spread in a beam of particles. The mean square lateral displacement, irrespective of angle, is given approximately by [1]

$$\langle y^2 \rangle = \frac{1}{2} \theta_s^2 L^2 \quad (2.96)$$

where  $L$  is the distance traversed into the scattering medium.

## 2.8 Other electromagnetic effects

A large number of additional electromagnetic effects have been investigated. In this section we will discuss two interesting phenomena that may have useful applications in certain circumstances: channeling and acoustic radiation.

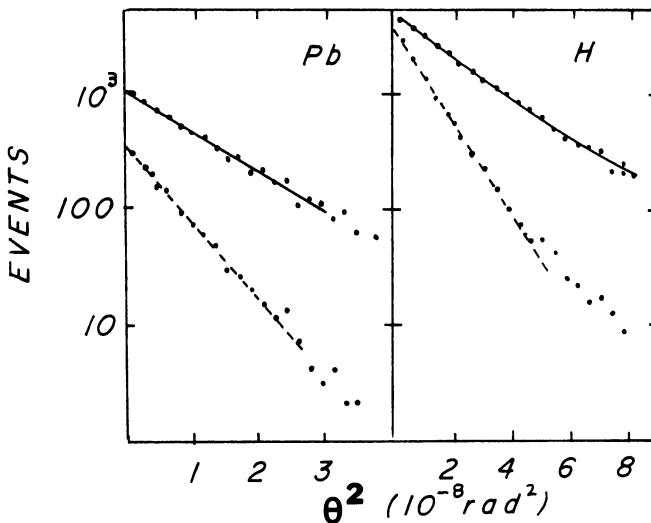
Until this point we have implicitly assumed that particles were passing through an amorphous material. In such a case each interaction is a random event, so that the results of multiple interactions are not correlated. The situation can be different, however, for crystals of materials such as silicon or germanium [26]. If the incident angle  $\psi_{\text{inc}}$  of the particle with respect to a low index, crystal axis is on the order of or smaller than the critical angle

$$\psi_{\text{crit}} = \sqrt{\frac{4Z_1Z_2e^2}{p_1v_1d}} \quad (2.97)$$

channeling effects may occur. The quantity  $d$  is the interatomic spacing along the channel, while  $p_1$  ( $v_1$ ) is the momentum (velocity) of the incident particle. For  $\psi_{\text{inc}} \lesssim \psi_{\text{crit}}$  the atoms of the crystal appear as an axial string. The correlated collisions with the string cause the particles to be gently attracted or repelled, depending on their charge. The atomic planes can have a similar steering effect.

Channeled positive particles tend to avoid the axial string. As a result, processes that are most important at small impact parameters tend to be suppressed. For example, channeled protons or  $\pi^+$  show smaller than random energy loss, reduced nuclear absorption, and reduced wide angle

**Figure 2.20** The distribution of  $\theta^2$  for 50-GeV/c negative hadrons in hydrogen and 70-GeV/c negative hadrons in lead. The lower curves show the distributions taken with the target removed. The solid curves are fits using the Moliere theory. (After G. Shen et al., Phys. Rev. D 20: 1584, 1979.)

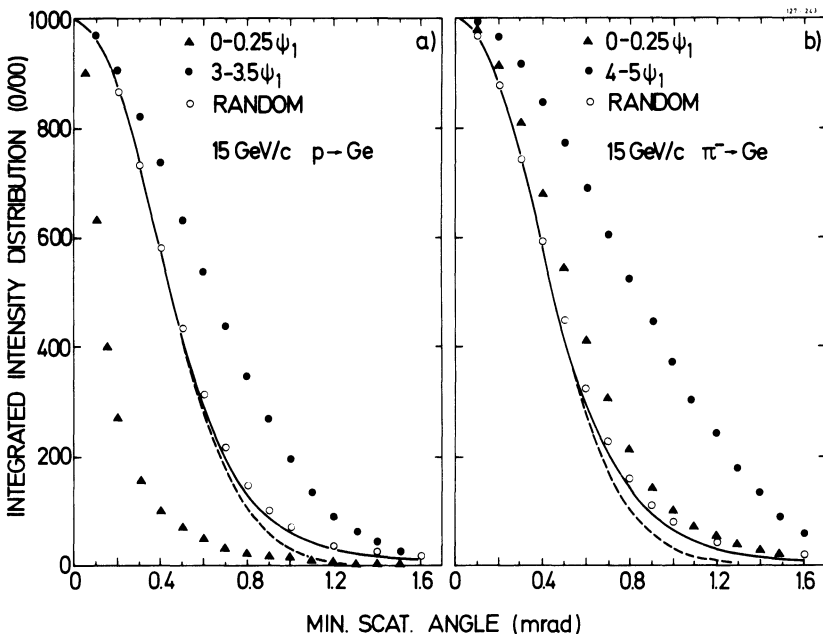


scattering and have a large transmission near  $\psi_{\text{inc}} = 0^\circ$ . Channeled  $\pi^-$ , on the other hand, are attracted to the string and show increased nuclear absorption, increased wide angle scattering, and a reduced transmission for  $\psi_{\text{inc}} \sim 0^\circ$ .

Channeling can also influence multiple scattering [27]. Figure 2.21 shows multiple scattering distributions for 15-GeV/c protons and  $\pi^-$ . The random scattering data agree well with the predictions of the Moliere theory. When  $\psi_{\text{inc}} < \psi_{\text{crit}}$  ( $\Delta$ ) the multiple scattering for protons is reduced, while that for  $\pi^-$  is increased. Interestingly, for  $\psi_{\text{inc}} \sim 3\psi_{\text{crit}}$  the multiple scattering for both charges is larger than for random scattering.

The oscillatory motion of channeled electrons and positrons leads to the emission of channeling radiation [26, 28]. This type of radiation has the same origin as ordinary bremsstrahlung, discussed in Section 2.4, and as coherent bremsstrahlung, which results when the incoming particle has periodic contacts with atoms in the target material. Ordinary bremsstrahlung differs from the other types of radiation because it has a continuous photon emission spectrum. In coherent bremsstrahlung the transverse

**Figure 2.21** Scattering angle distributions of 15-GeV/c p and  $\pi^-$  transmitted through a 4.2-mm-thick germanium crystal.  $\psi_1$  is the critical angle. (S. Andersen et al., Nuc. Phys. B 167: 1, 1980.)



motion of the incident particle is free, while in channeling radiation the transverse motion is bound by the potential of the atomic string.

In the channeling regime the intensity of the emitted radiation is enhanced over the ordinary bremsstrahlung by a factor proportional to  $\gamma^{1/2}Z_2^{-2/3}$ . Channeled radiation is emitted in the forward direction within a cone with characteristic half-angle  $\theta_c \sim \gamma^{-1}$ . The emitted photon frequency  $\omega$  and emission angle  $\theta$  in the LAB are related by

$$\omega \approx \frac{2\gamma^2\omega_0}{1 + \gamma^2\theta^2} \quad (2.98)$$

where  $\gamma\omega_0$  is the classical oscillation frequency for the electron or positron in its rest frame. Since the channeling radiation is linearly polarized, channeled beams of electrons or positrons may provide a useful source for a polarized photon beam. The emitted photon spectrum from incident electrons tends to be broader and show less structure than that from incident positron beams.

When a beam of particles is passed through a liquid, the deposited energy can cause the affected volume to undergo an adiabatic expansion. This in turn produces a detectable bipolar acoustic pressure wave [29]. The thermoacoustic model predicts that the time dependent pressure wave  $P(t)$  satisfies the equation

$$\int_{-\infty}^{\infty} tP(t) dt \approx -\frac{K}{4\pi C_p} \frac{E}{R} \quad (2.99)$$

where  $K$  is the volume coefficient of expansion and  $C_p$  is the heat capacity of the medium,  $E$  is the total deposited energy, and  $R$  is the distance to the observation point. The dependence of the acoustic signal on the quantities on the right-hand side of Eq. 2.99 was confirmed by experiments. The signal amplitude was linearly dependent on the deposited energy to within a factor of 2 for deposited energies between  $2 \times 10^{15}$  and  $4 \times 10^{20}$  eV. The signal amplitude in  $\text{CCl}_4$  was 24 times as large as the signal in  $\text{H}_2\text{O}$ , in rough agreement with the ratios of the values of  $K/C_p$ .

Some of the applications envisioned for acoustic radiation include a beam monitor, heavy ion detector, hadron calorimeter, or a cosmic ray detector. The primary advantage of the technique is that the hydrophones, which detect the acoustic pulses, are much less expensive than photomultiplier tubes or other common detectors. In addition, one can sample large volumes since the attenuation length of sound in liquids is long. The major disadvantage is the very low threshold required to

produce a signal. It is estimated that the ultimate detector threshold would be around  $10^{13}$  eV [29].

### References

- Some other general references not specifically cited below include Enrico Fermi, *Nuclear Physics*, Chicago: University of Chicago, 1950, Chap. 2; R. M. Sternheimer, Interaction of Radiation with Matter, in L. C. Yuan and C.-S. Wu, (eds.), *Methods of Experimental Physics*, New York: Academic, 1961, Vol. 5A, pp. 1–88.
- [1] An excellent introduction to the subject matter of this chapter can be found in B. Rossi, *High Energy Particles*, Englewood Cliffs: Prentice-Hall, 1952, Chap. 2. References 2 and 3 also contain much useful information.
  - [2] J. Jackson, *Classical Electrodynamics*, New York: Wiley, 1962.
  - [3] E. Segre, *Nuclei and Particles*, 2nd ed., Reading: Benjamin, 1977, Chap. 2.
  - [4] U. Fano, Penetration of protons, alpha particles, and mesons, *Ann. Rev. Nuc. Sci.* 13: 1–66, 1963.
  - [5] S. Ahlen, Theoretical and experimental aspects of the energy loss of relativistic heavily ionizing particles, *Rev. Mod. Phys.* 52: 121–73, 1980. This reference contains a nice summary of various investigators' contributions to the energy loss problem.
  - [6] The theory of the density effect correction is given by R.M. Sternheimer, The density effect for the ionization loss in various materials, *Phys. Rev.* 88: 851–9, 1952; the corrections have been updated using the latest data for the ionization potential in R.M. Sternheimer, S.M. Seltzer, and M.J. Berger, Density effect for the ionization loss of charged particles in various substances, *Phys. Rev. B* 26: 6067–76, 1982; erratum, *B* 27: 6971, 1983; and R.M. Sternheimer, M.J. Berger, and S.M. Seltzer, Density effect for the ionization loss of charged particles in various substances, *Atomic Data and Nuclear Data Tables* 30: 261–71, 1984.
  - [7] A. Walenta, J. Fischer, H. Okuno, and C. Wang, Measurement of ionization loss in the region of relativistic rise for noble and molecular gases, *Nuc. Instr. Meth.* 161: 45–58, 1979.
  - [8] J. Burq, M. Chemarin, M. Chevallier, A. Denisov, T. Ekelof, P. Grafstrom, E. Hagberg, B. Ille, A. Kashchuk, A. Kulikov, M. Lambert, J. Martin, S. Maury, M. Querrou, V. Schegelsky, I. Tkach, and A. Vorobyov, Observation of the ionization energy loss of high energy protons and pions in hydrogen gas, *Nuc. Instr. Meth.* 187: 407–11, 1981.
  - [9] R. Talman, On the statistics of particle identification using ionization, *Nuc. Instr. Meth.* 159: 189–211, 1979.
  - [10] H. Maccabee and D. Papworth, Correction to Landau's energy loss formula, *Phys. Lett.* 30A: 241–2, 1969.
  - [11] The parameters used in Vavilov's and others theories are presented in some detail in H. Bichsel and R. Saxon, Comparison of calculational methods for straggling in thin absorbers, *Phys. Rev. A* 11: 1286–96, 1975.
  - [12] H. Bethe and J. Ashkin, Passage of radiation through matter, in E. Segre (ed.), *Experimental Nuclear Physics*, Vol. 1, Part 2, New York: Wiley, 1959.
  - [13] Particle Data Group, Review of particle properties, *Phys. Lett.* 111B: 1, 1982.
  - [14] Y. Tsai, Pair production and bremsstrahlung of charged leptons, *Rev. Mod. Phys.* 46: 815–51, 1974.
  - [15] W. Heitler, *The Quantum Theory of Radiation*, 3rd ed., Oxford: Clarendon Press, 1953.

- [16] R. Siemann, W. Ash, K. Berkelman, D. Hartill, C. Lichtenstein, and R. Littauer, Wide angle bremsstrahlung, *Phys. Rev. Lett.* 22: 421–4, 1969.
- [17] J. Hubbell, Photon cross sections, attenuation coefficients, and energy absorption coefficients from 10 keV to 100 GeV, National Bureau of Standards report, NSRDS-NBS 29, 1969.
- [18] J. Eickmeyer, T. Gentile, S. Michalowski, N. Mistry, R. Talman, and K. Ueno, High energy electron-pair photoproduction from nuclei: Comparison with theory, *Phys. Rev. D* 21: 3001–4, 1980.
- [19] J. Bjorken and S. Drell, *Relativistic Quantum Mechanics*, New York: McGraw-Hill, 1964, Chap. 7.
- [20] R. Brandelik, W. Braunschweig, K. Gather, F.J. Kirschfink, K. Lubelsmeyer, H.-U. Martyn, G. Peise, J. Rimkus, H.G. Sander, D. Schmitz, D. Trines, W. Wallraff, H. Boerner, H.M. Fischer, H. Hartmann, E. Hilger, W. Hillen, G. Knop, L. Kopke, H. Kolanoski, R. Wedemeyer, N. Wermes, M. Wollstadt, H. Burkhardt, S. Cooper, J. Franzke, D. Heyland, H. Hultschig, P. Joos, W. Koch, U. Kotz, H. Kowalski, A. Ladage, B. Lohr, D. Luke, H.L. Lynch, P. Mattig, K.H. Mess, D. Notz, J. Pyrlík, D.R. Quarrie, R. Riethmüller, W. Schütte, P. Soding, G. Wolf, R. Fohrmann, H.L. Krasemann, P. Leu, E. Lohrmann, D. Pandoulas, G. Poelz, O. Romer, P. Schmuser, B.H. Wiik, I. Al-Agil, R. Beuselinck, D.M. Binnie, A.J. Campbell, P.J. Dornan, D.A. Garbutt, T.D. Jones, W.G. Jones, S.L. Lloyd, J.K. Sedgbeer, K.W. Bell, M.G. Bowler, I.C. Brock, R.J. Cashmore, R. Carnegie, P.E.L. Clarke, R. Devenish, P. Grossmann, J. Illingworth, M. Ogg, G.L. Salmon, J. Thomas, T.R. Wyatt, C. Youngman, B. Foster, J.C. Hart, J. Harvey, J. Proudfoot, D.H. Saxon, P.L. Woodworth, M. Holder, E. Duchovni, Y. Eisenberg, U. Karshon, G. Mikenberg, D. Revel, E. Ronat, A. Shapira, T. Barklow, T. Meyer, G. Rudolph, E. Wicklund, Sau Lan Wu, and G. Zoebnig, Electroweak coupling constants in the leptonic reactions  $e^+e^- \rightarrow e^+e^-$  and  $e^+e^- \rightarrow \mu^+\mu^-$  and search for scalar leptons, *Phys. Lett.* 117B: 365–71, 1982.
- [21] V. Highland, Some practical remarks on multiple scattering, *Nuc. Instr. Meth.* 129: 497–9, 1975; erratum, *Nucl. Instr. Meth.* 161: 171, 1979.
- [22] H. Bethe, Molière's theory of multiple scattering, *Phys. Rev.* 89: 1256–66, 1953.
- [23] W. Scott, The theory of small angle multiple scattering of fast charged particles, *Rev. Mod. Phys.* 35: 231–313, 1963.
- [24] A. Hanson, L. Lanzl, E. Lyman, and M. Scott, Measurement of multiple scattering of 15.7 MeV electrons, *Phys. Rev.* 84: 634–7, 1951.
- [25] G. Shen, C. Ankenbrandt, M. Atac, R. Brown, S. Ecklund, P. Gollon, J. Lach, J. MacLachlan, A. Roberts, L. Fajardo, R. Majka, J. Marx, P. Nemethy, L. Rossetet, J. Sandweiss, A. Schiz, and A. Slaughter, Measurement of multiple scattering at 50 to 200 GeV/c, *Phys. Rev. D* 20: 1584–8, 1979.
- [26] V. Beloshitsky and F. Komarov, Electromagnetic radiation of relativistic channeling particles (The Kumakhov effect), *Phys. Rep.* 93: 117–197, 1982.
- [27] S. Andersen, O. Fich, H. Nielsen, H. Schiott, E. Uggerhøj, C. Vraast Thomsen, G. Charpak, G. Petersen, F. Sauli, J. Ponpon, and P. Siffert, Influence of channeling on scattering of 2–15 GeV/c protons,  $\pi^+$ , and  $\pi^-$  incident on Si and Ge crystals, *Nuc. Phys. B* 167: 1–40, 1980.
- [28] J. Andersen, E. Bonderup, and R. Pantell, Channeling radiation, *Ann. Rev. Nuc. Part Sci.* 33: 453–504, 1983.
- [29] L. Sulak, T. Armstrong, H. Baranger, M. Bregman, M. Levi, D. Mael, J. Strait, T. Bowen, A. Pifer, P. Polakos, H. Bradner, A. Parvulescu, W. Jones, and J. Learned, Experimental studies of the acoustic signature of proton beams traversing fluid media, *Nuc. Instr. Meth.* 161: 203–17, 1979.



**Exercises**

1. Consider a 10-GeV/ $c$  proton incident on an aluminum target. Estimate the range of valid impact parameters for calculating  $dE/dx$ . Assume that  $\hbar\omega$  is approximately equal to the ionization potential for the atom.
2. What is the expected mean energy loss of 50-GeV/ $c$  protons in beryllium? How much is this result affected by the density effect correction?
3. Consider a 10-GeV/ $c$   $K^-$  beam in liquid hydrogen. What is the maximum kinetic energy of delta rays produced by the beam? How many delta rays with kinetic energy greater than 100 MeV are produced in 2 cm?
4. Calculate the Landau distribution function numerically and plot  $f_L(\lambda)$  versus  $\lambda$ .
5. Find the most probable energy loss of 100 GeV/ $c$   $\pi^-$  in copper. What is the probability of observing an energy loss of half of this amount and twice this amount?
6. Find the ionization energy loss of a 20-GeV positron in lead.
7. Find the cross section for a 30-GeV electron to undergo bremsstrahlung in a lead target and emerge with an energy of 25 GeV. Is the complete screening hypothesis justified?
8. Consider the Compton scattering of a 1-MeV photon. What is the energy of a photon scattered at  $30^\circ$ ? What is the kinetic energy and angle of the recoil electron?
9. Find the total pair production cross section for a 50-GeV photon in gold. What is the differential cross section for producing a 20-GeV electron? Is the complete screening hypothesis justified?
10. Plot the difference between the Moller and Bhabha differential cross sections as a function of  $\cos \theta^*$ .
11. Make a table showing the minimum and maximum angles of validity for Rutherford scattering and the total Coulomb cross section for 1-GeV protons in carbon, iron, and lead.
12. Find the Rossi–Greisen mean scattering angle  $\theta_s$  for 6-GeV  $K^-$

after traversing 2 cm of copper. How large is the Highland correction to  $\theta_s$ ?

13. Calculate numerically the Moliere scattering distribution for 10-GeV electrons after passing through 1 radiation length of lead. Plot  $\psi_{ms}$  as a function of  $\theta$ .
14. Estimate the critical angle for channeling of a 20-GeV/ $c$   $\pi^-$  in tin.
15. Use the data of Table 2.1 to check the validity of Bloch's expression for the ionization potential.